



The histone variant macroH2A1.1 regulates gene expression by direct association with their transcription start site

Ludmila Recoules, Alexandre Heurteau, Flavien Raynal, Fatima Moutahir, Fabienne Bejjani, Isabelle Jariel-Encontre, Olivier Cuvier, Anne-Claire Lavigne, Kerstin Bystricky

► To cite this version:

Ludmila Recoules, Alexandre Heurteau, Flavien Raynal, Fatima Moutahir, Fabienne Bejjani, et al.. The histone variant macroH2A1.1 regulates gene expression by direct association with their transcription start site. 2020. hal-03037462

HAL Id: hal-03037462

<https://hal.science/hal-03037462>

Preprint submitted on 3 Dec 2020

HAL is a multi-disciplinary open access archive for the deposit and dissemination of scientific research documents, whether they are published or not. The documents may come from teaching and research institutions in France or abroad, or from public or private research centers.

L'archive ouverte pluridisciplinaire **HAL**, est destinée au dépôt et à la diffusion de documents scientifiques de niveau recherche, publiés ou non, émanant des établissements d'enseignement et de recherche français ou étrangers, des laboratoires publics ou privés.

The histone variant macroH2A1.1 regulates gene expression by direct association with their transcription start site.

Ludmila Recoules¹, Alexandre Heurteau¹, Flavien Raynal¹, Fatima Moutahir¹,
Fabienne Bejjani³, Isabelle Jariel-Encontre³, Olivier Cuvier¹, Anne-Claire Lavigne^{1*}
and Kerstin Bystricky^{1,2*}.

¹ Laboratoire de Biologie Moléculaire Eucaryote (LBME), Centre de Biologie
Intégrative (CBI), Université de Toulouse, CNRS, UPS, F-31062 Toulouse, France.

² Institut Universitaire de France (IUF).

³ Institut de Génétique Moléculaire de Montpellier, CNRS, UMR5535, Equipe
Labellisée Ligue Nationale contre le Cancer, F-34293, France.

*Corresponding authors.

E-mails : kerstin.bystricky@ibcg.biotoul.fr ; anne-claire.lavigne@ibcg.biotoul.fr

Abstract

The histone variant macroH2A1 (mH2A1) is involved in cellular growth, differentiation and reprogramming, but the underlying molecular mechanisms are a matter of debate. Different roles of mH2A1 in gene expression may relate to functional differences of its two splicing isoforms, mH2A1.1 and mH2A1.2. Here, we map for the first time genome-wide localization of endogenous mH2A1.1 and link the distribution of mH2A1.1 to control of gene expression in human breast cancer cells. In addition to localization shared with mH2A1.2 to facultative heterochromatin, mH2A1.1 specifically associates with regulatory elements required for gene activation, super-enhancers and promoters of highly expressed genes. Depending on the recruitment profile of mH2A1.1 to these elements, selective depletion of mH2A1.1 up- or downregulates its target genes. mH2A1.1 represses transcription when its binding is spread over the entire gene and promoter, and activates transcription when its binding is strictly confined to the transcription start site (TSS). Notably, RNA Polymerase II was frequently in pause at mH2A1.1-activated genes. Functionally, mH2A1.1-dependent regulation of a subset of paused genes impedes mammary tumor cell migration. Molecular mechanisms of mH2A1.1 function at the TSS uncovered by our study define an intriguing new mode of transcription regulation in cancer cells.

Author Summary

Control of gene expression driving cellular functions from differentiation to epistasis and causing, when dysfunctional, uncountable diseases, relies on modifications of chromatin structure. One key element enabling chromatin plasticity is

the replacement of canonical histones by histone variants. Among histone variants macroH2A1 (mH2A) is an extraordinary H2A variant possessing a large non-histone domain placed outside of the nucleosome. Two splicing isoforms, mH2A1.1 and mH2A1.2, are produced, but these are rarely studied separately because they only differ in a 30 amino acid region and are difficult to distinguish experimentally, which likely explains contradictory functions reported in the literature. Here, we take advantage of a mH2A1.1 specific antibody to generate the first genome-wide chromatin-associated map of this histone variant in the invasive breast cancer cells line MDA-MB231. We confirm that mH2A1.1, like mH2A1.2, is enriched at facultative heterochromatin in agreement with its reported role as a repressor. However, we discovered that unlike its splicing isoform, mH2A1.1 specifically binds to super-enhancers and the transcription start site of highly transcribed genes. mH2A1.1 is necessary for regulating transcription of these genes. At the cellular level, we demonstrate that mH2A1.1 inhibits migration capacity of highly metastatic breast cancer cells. Our study characterizes for the first time binding profiles of mH2A1.1 that are linked to regulation of gene expression, thereby providing a new molecular mechanisms which govern the plasticity of human tumor cells.

Introduction

Compaction of DNA into chromatin modulates DNA accessibility, thereby regulating key molecular processes such as transcription [1,2]. Histone post-translational modifications, chromatin-remodeling enzymes, DNA-binding factors and architectural proteins fine-tune genome organization and dynamics [1,2]. In addition, histone variants replace canonical histones in a locus-specific manner, which endows

chromatin with additional properties required to regulate DNA accessibility and functions [3].

Among the histone variants, macroH2A1 (mH2A1) is a vertebrate-specific [4,5] histone H2A variant composed of an N-terminal H2A-like domain (64 % identical to H2A) and a C-terminal 25 kDa ‘macro’ domain. These two domains are joined by an unstructured 41 amino acid long linker that positions the macro domain outside of the nucleosome [6]. Expression of the highly conserved *H2AFY* gene produces two splicing isoforms, mH2A1.1 and mH2A1.2, whose sequences differ in a 30 amino-acid region within the macro domain [6].

mH2A1 was originally found to be enriched on the transcriptionally silent X chromosome [7]. mH2A1 is also present at autosomes, forming large domains in association with histone marks associated with heterochromatin, such as H3K27me3 and H3K9me3 [8–10]. *In vitro* studies have demonstrated that nucleosomal mH2A1 interferes with binding of the transcription factor NFκB, and inhibits nucleosome sliding by the remodeling complex SWI/SNF and initiation of RNA polymerase II (Pol II) transcription [11,12]. Therefore, mH2A1 is believed to play a role in transcriptional repression. However, in a few cases the presence of mH2A1 has been seen to correlate with active transcription of a subset of genes involved in a variety of processes such as cell differentiation, lipid metabolism and cell-cell signaling [8,13–17]. Thus, the roles of mH2A1 in regulating gene expression are seemingly contradictory. Studying mH2A1 isoforms separately may help to better understand their roles.

The two mH2A1 splice variants exhibit tissue- and cell-specific expression patterns[18]. In normal cells, the mH2A1.2 isoform appears ubiquitously expressed [19–21]. Mainly incorporated into heterochromatin (X-inactive chromosome and

autosomic heterochromatin) [7–9,22], this splicing isoform is generally associated with gene repression. However, a few recent studies discovered that mH2A1.2 was required for gene expression. Indeed, in mouse muscle cells [13], mH2A1.2 binds muscle-specific enhancers necessary for the activation of the myogenic regulator network. In human embryonic stem cells (hESCs) [23], binding of mH2A1.2 to gene promoters seems to control gene expression both positively and negatively. However, the binding profile of mH2A1.2 in hESC was not conserved in mesoderm-derived human fibroblasts [23].

In contrast to mH2A1.2, mH2A1.1 is only expressed in differentiated cells with low proliferation rates [19–21]. In tumors, expression of the mH2A1.1 isoform is frequently reduced, as compared to normal tissues, suggesting that this isoform is a tumor suppressor [20,21,24]. In highly metastatic cancers such as triple-negative breast cancers however, expression levels of mH2A1.1 are increased and correlate with poor prognosis [24].

Only mH2A1.1 can bind NAD⁺ metabolites through its macro domain [25] and interact with the DNA-damage repair and chromatin remodeling factor PARP1 (Poly(ADP-Ribose) Polymerase 1) [14,26–28]. Interaction between mH2A1.1 and PARP1 seems to be key for the capacity of mH2A1.1 to regulate DNA damage responses [29,30], mitochondrial respiration [28] and gene transcription [14,27,31]. In particular, it was proposed that mH2A1.1 and PARP1 recruit CBP (CREB-binding protein) to mediate acetylation of H2BK12/K120 and to regulate, in part, mH2A1-target gene expression in IMR90 cells, without really demonstrated the specific action of mH2A1.1 with respect to mH2A1.2 [14]. In other hand, recruitment of mH2A1.1 to repressed signal-inducible genes is required for their stress response [31,32]. Despite this knowledge about functions of mH2A1.1, neither its chromatin

association, independently of the one of mH2A1.2, nor its specific mechanisms of action during gene activation, was clearly analyzed.

To gain a better understanding of the roles of mH2A1.1 in regulating gene expression, we determined 1) the genomic localization of mH2A1.1 and 2) its effect on gene expression. To that end, we generated a ChIP-grade mH2A1.1-specific antibody. Chromatin immunoprecipitation followed by sequencing (ChIP-seq) of mH2A1.1, of total mH2A1 and of a variety of histone marks, shows that both mH2A1 isoforms bind to heterochromatin and to enhancers. Surprisingly, only the mH2A1.1 isoform binds TSSs (Transcription Start Site) of active genes. Interestingly, we show that mH2A1.1-activated genes are mostly Pol II paused genes. Frequently, these genes are negatively implied in cell migration in mammary tumor cells. We demonstrate that mH2A1.1 impedes cell migration whereas mH2A1.2 promotes it. Our work describes a novel gene activation pathway in cancer cells dependent on the selective recruitment of mH2A1.1 to the TSS of paused genes.

Results

mH2A1.1 and mH2A1.2 preferentially associate with facultative heterochromatin. We determined the genomic localization of mH2A1.1 in the claudin-low breast cancer cell line MDA-MB231 which expresses this histone variant at a high level compared to other types of breast cancer cell lines (S1A, S1B Fig) [24]. To that end, we developed a ChIP-grade polyclonal rabbit antibody that exclusively recognizes mH2A1.1 (Ab α mH2A1.1) (S1C-S1F Fig) By ChIP-seq, we determined the distribution of mH2A1.1 and of total mH2A1 using Ab α mH2A1.1 and

a commercially available ChIP-grade antibody (Ab37264 (Ab α mH2A1)) (S1, S2 Tables and S1G-S1I Fig), respectively.

We identified 29,112 peaks for mH2A1.1 (Ab α mH2A1.1) and 22,789 peaks for total mH2A1 (Ab α mH2A1), covering combined 13.6 % of the genome. Genome-wide, ChIP-seq results obtained with these two antibodies were highly similar with a significant co-occurrence of peaks (Fisher exact test (FET): p-value $< 2.2 \times 10^{-16}$ and Odd ratio = 27.40) and a Pearson coefficient correlation (PCC) of 0.92 (S2A Fig).

Analysis of peaks detected with Ab α mH2A1 and Ab α mH2A1.1 shows that regions occupied by mH2A1.1 and mH2A1.2 do not overlap completely (Fig 1A) suggesting that some regions are preferentially bound by either one of the variants. Indeed, a significant number of sites (18,838) is preferentially recognized by Ab α mH2A1.1 and not by Ab α mH2A1 (Fig 1A). Of note, Ab α mH2A1 has lower efficacy than Ab α mH2A1.1 in detecting mH2A1.1 and may, when reducing detection thresholds, recognize a fraction of these sites (S1B, S1G, S1H Fig). Genomic regions common to both antibodies correspond to one or more peaks exclusively recognized as mH2A1.1 or both isoforms in unknown relative proportions. For further analysis, we defined three types of genomic regions: regions incorporating preferentially only mH2A1.1 (mH2A1.1 only), regions incorporating preferentially only mH2A1.2 (mH2A1.2 only) and regions incorporating either mH2A1.1 or both isoforms (mH2A1s) (Fig 1A).

These ChIP-seq results raise the possibility that preferential genomic localization of the mH2A1.1 variant relate to its function. To test this possibility, we first characterized the distribution of mH2A1.1 ChIP-seq peaks with respect to selected genomic features (Fig 1B; see Materials and Methods). Nearly one third of

mH2A1.1 peaks were associated with distal intergenic regions and another third of mH2A1.1 peaks with promoters (TSS \pm 1kb) (Fig 1B).

Next, we analyzed mH2A1.1 genomic localization with respect to the chromatin environment of the identified regions. We first integrated ENCODE ChIP-seq of heterochromatin histone marks (H3K9me3 and H3K27me3) [33]. We found that genome-wide, mH2A1.1 ChIP-seq peaks were significantly enriched with the H3K27me3 repressive histone mark, in a manner comparable to the one observed using Ab α mH2A1 (Figs 1C and S2A). We confirmed the enrichment of mH2A1.1 on heterochromatin domains in independent ChIP-qPCR experiments on WT and mH2A1.1-deficient cells using two different siRNAs directed against mH2A1.1 isoform (S3A-S3E and S4 Figs). Remarkably, even if the related PCCs were low between H3K9me3 and mH2A1 isoforms (S2A Fig), in particular for mH2A1.1, we detected that both mH2A1 isoforms overlapped significantly with H3K9me3 (Fig 1C). At heterochromatin domains (i.e. marked by H3K27me3 and/or H3K9me3), both mH2A1 ChIP-seq peaks were highly similar with a PCC of 0.94 (S2B Fig). Surprisingly, 80% of H3K27me3 overlapped with H3K9me3 (Fig 1C), although often presented as non-overlapping heterochromatin histone marks [34]. However, within peaks common to H3K27me3 and H3K9me3, the contribution of each mark was inversely proportional (Figs 1D and S5A). In addition, a high H3K27me3 to H3K9me3 ratio was more associated with genes whereas low H3K27me3 to H3K9me3 ratio was more associated with gene-poor genomic regions (Fig 1D and S5B). Hence, in this cell line, levels of relative enrichment between H3K27me3 and H3K9me3 could be used to distinguish “facultative-like” heterochromatin (with high levels of H3K27me3 and low levels of H3K9me3), from “constitutive-like” heterochromatin (with low levels of H3K27me3 and high levels of H3K9me3). In this context, we

observed that the genomic distribution of both mH2A1 isoforms positively correlates with regions rich in H3K27me3 and poor in H3K9me3 levels, hence corresponding to “facultative-like” heterochromatin (Fig 1E).

mH2A1.1 binds to super-enhancers. Because a large number of mH2A1.1 sites are associated with promoter regions (Fig 1B), we performed ChIP-seq experiments for a panoply of histone marks usually associated with active transcription (H3K4me1, H3K4me3, H3K27ac and H3K36me3) (*Bejjani et al, in preparation*). We found that mH2A1.1 correlated positively with H3K4me1 and H3K27ac, two chromatin modifications which characterize active enhancer regions [35] (Figs 2A and S2A). We found that more than 40% of mH2A1.1 and total mH2A1 overlapped significantly with “putative” enhancers outside of TSSs (Fig 2B; see Materials and Methods). 17% of “putative” enhancers were bound by mH2A1 isoforms. Among them, some were common to mH2A1.1 and total mH2A1 (48%) but many were only bound by mH2A1.1 (33%) or by mH2A1.2 (19%). At “putative” enhancers, both mH2A1 ChIP-seq results were still similar with a PCC of 0.80 (S2B Fig). Interestingly, mH2A1-bound regions frequently formed large domains comprising a group of enhancers marked with H3K27ac (Fig 2C), which could correspond to super-enhancers (SE) [36,37]. Using the ROSE package to detect SEs marked by the H3K27ac signal [36,37], we identified “putative” SEs in MDA-MB231 cells (Materials and Methods). We show that 85% of these SEs were bound by at least one mH2A1 isoform, 19% of them were associated with mH2A1.1 compared to only 3% with mH2A1.2 only (Fig 2D). The enrichment of mH2A1.1 at super-enhancers was confirmed in independent ChIP-qPCR experiments in WT and mH2A1.1-deficient

cells using two different siRNAs directed against the mH2A1.1 isoform (S3A-S3E and S4 Figs).

mH2A1.1 binds to the transcription start site of active genes. A striking genomic feature identified for mH2A1.1 was its binding to TSSs (+/- 1kb) (hereafter referred to as “promoter regions”) (Fig 1B) confirmed by independent ChIP-qPCR experiments in WT and mH2A1.1-deficient cells by two different siRNAs directed against mH2A1.1 isoform (S3A-S3E and S4 Figs). Therefore, we characterized the association of mH2A1 isoforms at these genomic sites in more detail. Our ChIP-seq data showed that mH2A1.1 was more frequently associated with promoter regions than mH2A1 (41% vs 35%, respectively) (Fig 3A). Interestingly, among promoter regions bound by mH2A1 isoforms, 45% of them were occupied by mH2A1.1 only, whereas 14% were occupied by mH2A1.2 only (Fig 3A). We thus wondered whether the chromatin environment of promoter regions correlates with specific binding of either isoform. At promoter regions, we found that mH2A1.1 positively correlated with active marks (H3K4me3 and Pol II) whereas mH2A1 positively correlated with repressive histone marks (H3K27me3 and H3K9me3) (S6A Fig). Interestingly, this difference in localization identified by the two antibodies was maintained when we considered the two genomic populations specific to each antibody, mH2A1.1 only and mH2A1.2 only (S6B, S6C Fig). These results strongly suggest that mH2A1.2 preferentially binds to promoters in a closed chromatin state whereas mH2A1.1 is mainly recruited to promoters in an open chromatin state. In agreement, at promoter regions, both mH2A1 ChIP-seq experiments differed from one another with a PCC of 0.41 (in comparison to a PCC of 0.92 genome-wide) (S2A, S2B Fig). To assess whether mH2A1.1 binding at the TSS correlates with transcription levels, we

generated RNA-seq data from MDA-MB231 cells. We then stratified genes into four equal categories according to their expression levels (from silent to highly expressed genes). We determined the distribution of both mH2A1 isoforms at the TSS (\pm 2 kb) and over the gene body (region from the TSS to the Transcription End Site (TES)) for those four groups of genes (see Materials and Methods). We found that the amount of mH2A1.1 bound to TSSs increased with expression levels while relative amounts recruited onto gene bodies decreased (Figs 3B, 3C and S7A-S7D). On the contrary, mH2A1 bound uniformly to TSSs and over the gene body of silent genes and its presence was restricted to the proximal promoter regions (around 1kb upstream TSSs) and downstream of TESs of expressed genes (Figs 3B, 3C and S7A-S7D). In agreement, mH2A1.1 peaks were mainly present at the TSS \pm 1kb of highly transcribed genes (Fig 3D), while mH2A1 peaks were present on the TSSs \pm 1kb of silent genes (Fig 3D). Similar observations were seen for active and repressive histone marks (S7E Fig). Here again, this difference in localization identified by the two antibodies was even stronger when we considered the two genomic populations specific to each antibody, mH2A1.1 only and mH2A1.2 only (Fig 3D). Notably, we observed that mH2A1.1 binding at TSSs was distributed uniformly around TSSs, peaking at maximum Pol II binding (Fig 3E). In agreement, at TSSs, 70% of mH2A1.1 peaks (two third of them being mH2A1.1 only) overlapped significantly with Pol II (Fig 3F), with a PCC of 0.48 (in comparison to a PCC of 0.07 genome-wide) (S2A and S7F Figs). Coherent with these results, mH2A1.2 only peaks were hardly detectable (3%) at Pol II TSS-bound sites (Fig 3F), and at TSSs, both mH2A1 ChIP-seq are anti-correlated with a PCC of -0.07 (S2B Fig). These results highlight highly specific association of the mH2A1.1 variant with the TSSs of transcribed genes.

mH2A1.1 regulates gene expression. Binding of mH2A1.1 to TSSs of transcribed genes prompted us to test whether mH2A1.1 was required for modulating gene expression. We generated RNA-seq data from MDA-MB231 cells in which mH2A1.1 protein expression was reduced by around 90 % by siRNA without significantly affecting expression of the mH2A1.2 isoform (S3A-S3C Fig). 533 genes (56.3%) were down-regulated (mH2A1.1-activated genes) and 412 genes (43.7%) were up-regulated (mH2A1.1-repressed genes) in mH2A1.1 knock-down (mH2A1.1 KD) conditions compared to WT conditions (Fig 4A, S8A and S3 Table). Altered gene expression was confirmed by RT-qPCR on a subset of genes using two different siRNAs directed against the mH2A1.1 isoform (S3 Fig). We found that all mH2A1.1 regulated genes, activated- as well as repressed- genes, were active or even highly expressed genes in WT conditions (S8B and S8C Fig). Strikingly, we revealed that mH2A1.1 and mH2A1 binding differed between mH2A1.1-activated and repressed genes (Figs 4B-4D and S9A). Indeed, mH2A1.1 was mainly bound upstream of the TSS and within the gene body of mH2A1.1-repressed genes. At mH2A1.1-activated genes, however, mH2A1.1 exclusively associated with the TSSs and upstream (up to 1kb) (Figs 4B-4D and S9A). mH2A1 was bound upstream and downstream of the TSS of mH2A1.1-repressed genes, whereas its level was at its lowest at the TSS. In contrast, its relative enrichment was very low at mH2A1.1-activated genes, with its highest levels upstream TSS (up to 1 kb) (Figs 4B-4D and S9A). Overall, these results suggest that mH2A1.1 promotes transcription when its binding is restricted to TSSs and represses transcription when its binding is spread over genes.

mH2A1.1 regulates expression of paused genes. We noted that Pol II was bound to the TSSs of mH2A1.1-activated genes but was barely detected on the

corresponding gene bodies (Figs 4B-4D and S9A). This pattern of Pol II distribution raised the possibility that mH2A1.1-activated genes may be in pause. To confirm this, we calculated the Pol II pausing index (PI) for transcribed genes using Pol II ChIP-seq data as described in [38] (see Materials and Methods). To see if the binding of mH2A1.1 at TSSs was related to the level of Pol II pausing, we first plotted the mH2A1.1 ChIP-seq signal around the TSS +/- 10 kb for each gene ranked by their PI (Fig 5A). We observed that confinement of mH2A1.1 to the TSS and its absence from the gene body is a characteristic of genes with a high PI. Genes where mH2A1.1 was spread along the entire gene body were characterized by low PIs (Fig 5A). In agreement, we found that mH2A1.1 peaks, as well as Pol II ones, were significantly sharper at the TSS (TSS +/- 1kb) of genes with a high PI as opposed to genes with a low PI (Figs 5B, 5C and S9B). Moreover, 40% of genes bound by mH2A1.1 only at the TSS have a PI > 2 and 31% of paused genes (defined as genes with PI>2, n=6,821) have mH2A1.1 only peaks at their TSS (Fig 5D). Furthermore, the correlation between mH2A1.1 binding and activation of paused genes appeared to be functionally relevant because the majority of mH2A1.1-activated genes (68%) have a pausing index greater than 2 and their PI are significantly higher than that of any other gene category tested (Fig 5E and 5F). In contrast, the majority of mH2A1.1-repressed genes (69%) was characterized by a PI < 2. These results suggest that mH2A1.1 spreading over the gene body represses genes whose expression is independent of Pol II pausing, whereas mH2A1.1 restricted to the TSS activates genes whose expression is dependent of Pol II pausing. Altogether, our results provide the first evidence of a functional link between the binding of mH2A1.1 at TSSs and Pol II pausing at promoter proximal regions. We propose that the

association of mH2A1.1 with the TSSs of a subset of paused genes enhances their transcription.

mH2A1.1 inhibits cell migration in MDA-MB231 cells. We found that genes de-regulated by the loss of mH2A1.1 were involved in four main processes: cell cycle, DNA repair, cytoskeleton organization and cell adhesion (S10A, S10B Fig and S4 Table). The two first processes were expected based on earlier studies [21,29,30,39]. However, the relationship between mH2A1.1 and expression of genes involved in cytoskeleton organization or cell adhesion was undocumented. Using a standard wide-field microscope, we observed that cells became more elongated after transfecting two different siRNA against mH2A1.1 (Fig 6A and 6B). We used a siRNA against mH2A1.2 (S3A-S3C Fig) to test whether this effect was specific of mH2A1.1. Interestingly, we observed that mH2A1.2 KD cells became rounder compared to control cells (Fig 6A-6B). Importantly, we noticed that numerous mH2A1.1 KD de-regulated genes modulate cell migration (examples of anti-migratory genes: ARRDC3 [40], SOCS4 [41], HACE1 [42] and FBXL4 [43] - and of pro-migratory genes: EIF6 [44], MT1E [45], JUND [46] and DAPK3 [47]). Thus, we investigated the effect of mH2A1.1 and mH2A1.2 depletion on the migratory capacity of MDA-MB231 cells using a Boyden Chamber assay (see Materials and Methods). Upon depletion of mH2A1.1, the migratory capacity of MDA-MB231 cells was significantly increased compared to control cells. In contrast, depleting the mH2A1.2 isoform led to a decrease in cell migration (Fig 6C and 6D). Strikingly, mH2A1.1-activated genes involved in cytoskeleton organization and cell adhesion were also amongst genes with a high Pol II pausing index (Fig 6E; see Materials and Methods). Taken together,

these results suggest that mH2A1.1 inhibits cell migration by in part enhancing the expression of paused genes involved in cytoskeleton organization and cell adhesion.

Discussion

In this study, we present the first map of the histone variant mH2A1.1 genomic distribution over the entire human genome in breast cancer cells. Integration of this map with chromatin features confirms that mH2A1.1, together with its splice variant mH2A1.2, localizes to “facultative-like” heterochromatin domains and enhancers. Importantly, for the first time in cancer cells, we identify a direct link between mH2A1.1 recruitment of transcribed genes and their transcriptional regulation. The impact of this recruitment on the transcriptional rate is functionally dichotomous, with positive or negative effects. This bivalence correlates with a differential distribution of mH2A1.1 around the TSS as well as to the level of dependency of the transcribed gene to the Pol II pausing.

The results of our mH2A1 ChIP-seq analysis are overall consistent with previously published reports identifying this histone variant as a widespread chromatin feature on autosomes, covering large domains, with a preferential recruitment to H3K27me3-decorated “facultative-like” heterochromatin (Fig 1C) [8,9,14,48]. Our mH2A1.1 ChIP-seq analysis allows us to show that even if mH2A1.1 distribution is mainly reminiscent of that of mH2A1.2, each variant has also specific heterochromatin localizations. Genome mapping of mH2A1.2 is not yet possible due to the poor specificity or lack of precipitation efficacy of commercial antibodies.

We further demonstrate that mH2A1.1-bound chromatin co-localizes significantly with the H3K9me3 histone mark (Fig 1C). A fraction of these sites are devoid of H3K27me3 and could correspond to the recently identified macroH2A localization at constitutive heterochromatin⁸. However, the vast majority of mH2A1.1-bound H3K9me3-decorated chromatin contained also tri-methylated H3K27 (Fig 1C). This difference may be a feature of the MDA-MB231 cell line, a high migratory capacity cancer cell line in which there is an abnormal expansion of frequently overlapping H3K9me3 and H3K27me3 marks along the genome [49,50].

Moreover, we noted that even though mH2A1.1 associates with heterochromatin domains, its partial loss alone is not sufficient to reactivate silenced genes present in these domains (S8 Fig). Similarly, even if mH2A1 binding was shown to overlap with H3K27me3 modified chromatin in primary human cells, no enrichment of H3K27me3 at mH2A1-regulated genes was observed [14]. Furthermore, mH2A1.2-occupied and repressed target genes are not reactivated upon mH2A1.2 knock-down [13]. These observations suggest that enrichment of both mH2A1 isoforms in heterochromatin domains may serve as a lock to conserve heterochromatin stability and architecture [9].

In parallel, we show that the depletion of mH2A1.1 alone is sufficient to alter the expression of many genes present in chromatin domains devoid of H3K27me3 (Figs 4A and S8C). Previous work identified a role for mH2A1.1 in the transcriptional rate of genes encompassed in H2B acetylated regions but this mechanism was described as specific of primary cells and absent from cancer cells [14]. Here, we demonstrate that the effect of mH2A1.1 depletion correlates with the distribution of mH2A1.1 along transcribed genes. Indeed, mH2A1.1 binding is restricted to the

TSSs of mH2A1.1-activated genes while mH2A1.1 binds both upstream and on the gene body of mH2A1.1-repressed genes (Fig 4B). Our findings reinforce the notion that mH2A1.1 has a dual role in gene regulation and this seems to depend on its distribution on mH2A1.1-regulated genes [14]. Molecular mechanisms determining mH2A1.1 differential localization and the consequent effects on gene regulation should now to be determined. Perhaps, mH2A1.1 post translational modifications favor binding to the TSS of active genes. Indeed, mH2A1-S137 phosphorylation excluded mH2A1 from the inactive X chromosome [51]. Specific protein partners could also be involved in the recruitment of mH2A1.1 to the TSSs of transcribed genes, for instance PARP1. Indeed, association of mH2A1.1 and PARP1 was shown to be involved in gene transcription, DNA repair and global cellular metabolism [14,18,29].

The vast majority of mH2A1.1 narrow peaks at TSSs was only recognized by our home-made antibody Ab α mH2A1.1 (Fig 3). We think that this is certainly due to the high affinity of Ab α mH2A1.1 towards mH2A1.1 compared to Ab α mH2A1 (S1F-S1H Fig). The quantity of mH2A1.1-restricted to the TSSs is significantly smaller than in the large domains, such as heterochromatin and SEs (Figs 1D,2C and 3C). Therefore, Ab α mH2A1 is certainly less efficient in immunoprecipitating mH2A1.1 in this context. Having a high affinity antibody led us to investigate new localizations and functions of the mH2A1.1 isoform. Now, it will be interesting to have a high affinity antibody against mH2A1.2. Indeed, through native-ChIP-seq experiments using a mH2A1.2 custom-made specific antibody, Dimitris Thanos and his collaborators recently showed that mH2A1.2 binds to the TSSs of transcribed genes in human embryonic stem cells [23]. Thus, adapted sequencing techniques, isoform-specific antibodies and appropriate extractions of mH2A1 chromatin sub-complexes

will enable studying mH2A1 splicing isoforms in different chromatin- and cell-dependent contexts.

Interestingly, we remarked that mH2A1.1 TSS-binding is distributed in a uniform manner around the TSS placing the maximum binding to the nucleosome free region (NFR) (Fig 3E). Its localization around the TSSs was also observed for mH2A1.2 using Native ChIP-seq [23], eliminating the hypothesis of a technical bias. The long- and unstructured- linker domain places the macro domain of mH2A1 outside nucleosomes [6]. Because antibodies against mH2A1 frequently recognize the linker or the macro domain (as Ab α mH2A1.1 and Ab α mH2A1, respectively), we hypothesize that mH2A1.1 is incorporated at the two adjacent nucleosomes of the TSSs but their macro domain could be joined at the NFR, which could explain the higher signal at the NFR compared to the two adjacent nucleosomes. Future analysis will be necessary to confirm this hypothesis.

At the cellular level, we observed that the silencing of mH2A1.1 promotes cell migration, whereas mH2A1.2 silencing increases migration in the MDA-MB231 breast cancer cell line. mH2A1 has been shown to be involved in cell migration in mouse [52,53] and human [52–55] models. The opposite roles of both splice variants on the migratory capacities that we see are in agreement with observations in previous studies using gastric cancer cells [55] and MDA-MB231 cells [52]. At the molecular level, the selective incorporation of mH2A1.2 along the SOD3 gene (playing a part in cell migration) has been shown to be directly linked to gene repression in mouse metastatic cells [52]. Here, we show that the migratory capacities of human metastatic breast cancer cells are directly regulated by selective recruitment of mH2A1.1. Among mH2A1.1-activated genes were genes responsible

for inhibiting cell migration. Thus, it is tempting to speculate that the negative effect of mH2A1.1 on cell migration is due to mH2A1.1-dependent activation of genes inhibiting migration. Interestingly, even if mH2A1.2 is very similar to mH2A1.1 in terms of amino-acid sequence, it has an opposite function to mH2A1.1 in the regulation of cell migration. Possibly the NAD⁺ metabolite binding pocket of mH2A1.1 plays a role in directing function. Here, we decipher in part the molecular mechanism by which mH2A1.1 could inhibit cell migration. Taken together, our data reveals antagonistic cellular functions of both mH2A1 isoforms and highlight the need to distinguish these isoforms when studying the role of mH2A1.

We demonstrate that mH2A1.1 favors expression of paused genes (70% of mH2A1.1-activated genes) (Fig 5E). It will be now interesting to dissect the molecular mechanisms that allow mH2A1.1 to promote transcription of paused genes. Perhaps, mH2A1.1 binding to the TSS could stimulate the recruitment of P-TEFb (Positive Transcription Elongation Factor) and consequently allow Pol II release [38]. PARP1, well known partner of mH2A1.1, is also involved in Pol II pausing release by mediating ADP-ribosylation of NELF (Negative elongation factor) [56] and could be recruited by mH2A1.1. This hypothesis could also explain why we observed mH2A1.1 at the TSS of highly transcribed genes (Fig 3B and 3D). The presence of mH2A1.1 at SEs could also induce Pol II release (Fig 2C and 2D). SEs are involved in cellular identity through the regulation of key genes involved in cellular identity [36,57]. Furthermore, SEs are known to play an important part in many diseases, including several cancers^{51–53} in which they drive expression of oncogenes [37,58]. To note, several clinical trials already utilize SE blockers (bromodomain and extra-terminal motif (BET) inhibitor and CDK7i) [59]. Among them, BRD4, one of the BET

protein family members, was targeted. BRD4 binds acetylated histones at TSSs and SEs, brings them together, and mediates transcriptional activation and elongation by RNA Pol II [37,58]. Interestingly, we observed that 74% of SEs are bound by mH2A1.1 and BRD4 in MDA-MB231 cells (*data not shown*). Could the presence of mH2A1.1 at SEs and TSSs be involved in the recruitment of BRD4 to enable elongation of RNA Pol II on paused mH2A1.1-activated genes ?

Overall, we demonstrate for the first time that mH2A1.1 activates transcription of paused genes by its selective recruitment to their TSSs. It remains to demonstrate whether mH2A1.1 is directly involved in the recruitment of factors acting on Pol II pausing events and/or on the establishment of 3D-chromatin structures (e.g chromatin looping mechanisms), facilitating Pol II pausing release.

Materials and Methods

Cell culture. MDA-MB231, HEK-293T and MCF7 cell lines were purchased from ATCC, and were maintained and amplified in Dulbecco's Modified Eagle's (DMEM) for HEK-93T and MDA-MB231 cells, and in DMEM-F12 for MCF7 cells, supplemented with gentamycin (50 µg/ml) (Gibco), fetal bovine serum (10%, Gibco) and sodium pyruvate (100 mM, Sigma). Cells were maintained in a humidified incubator at 37°C with 5% CO₂. Cells lines were regularly tested for mycoplasma infection (MycoAlert, Lonza). In Montpellier, MDA-MB231 cells were cultured in DMEM supplemented with 10% fetal calf serum and penicillin/streptomycin (100 µg/ml each) and regularly tested for mycoplasma infection.

Transfection of siRNAs and plasmids. At 30-50% cell confluence, transfection of siRNA (11nM) was performed using INTERFERin (Polyplus-Ozyme) according to the manufacturer's protocol. Cells in control condition were transfected with INTERFERin without any siRNA. Transfection of plasmid (1µg) was done with FuGene HD (Promega) according to the manufacturer's protocol. siRNA and plasmid sequences are available in S5 Table. Two and three days post plasmid and siRNA transfection respectively, cells were recovered for experiments.

Western blotting. Cells were lysed and subjected to western blot analysis as previously described [60]. Briefly, proteins extracts were separated in 10% polyacrylamide (1:125 bisacrylamide:acrylamide) SDS gels, transferred onto nitrocellulose membrane (Bio-Rad) and blocked with PBS-Tween 0.4% - Milk 5% for 1h at RT with rotation. Membranes were then incubated with primary antibodies overnight (O/N) at 4°C in PBS-Tween 0.4% - Milk 5% with rotation (or 1h30 at RT). Primary antibodies are described in the S1 Table. Membranes were next incubated with secondary antibody in PBS-Tween 0.4% - Milk 5% 1h at RT with rotation and the signal was detected using chemiluminescence. Secondary antibodies are described in the S1 Table. Signal quantifications were carried out with Image Lab software (Bio-Rad).

RNA extraction, reverse transcription and quantitative real-PCR (qRT-PCR). Total RNA was isolated using the RNAeasy midi kit (Qiagen). Purified RNA was reversed transcribed to cDNA using Maxima H Minus first Strand cDNA synthesis kit (Promega). The sequences of the primers used are available in S6 Table. RT-PCR was performed using iTaq Universal SYBR Green (Bio-Rad) according to manufacturer's instructions. At least two independent experiments were performed

for each condition. The relative expression levels of mRNA were normalized to RPLP0 mRNA expression and evaluated according to the $2^{-\Delta\Delta C_t}$ method [61].

Fluorescence microscopy. Two or three days post-transfection, cells were fixed with 4 % paraformaldehyde for 15 min for MDA-MB231 cells and 10 min for HEK-293T at RT. Cells permeabilization was carried out using 0.1 % Triton X-100 in PBS for 10 min at RT. Cells were then blocked with 5 % BSA-0.15% Tween in PBS for 1h at RT. Next, cells were incubated with primary antibody O/N at 4°C. Cells were then incubated with Alexa conjugated secondary antibody for 1h at RT. Actin was labelled using cytoPainter Phalloidin iFluor diluted 1:1000 with secondary antibody according to the manufacturer's protocol (Abcam; see S1 Table). Antibodies references and dilutions are provided in S1 Table. The coverslips were finally incubated with Hoechst (Invitrogen, 33342) for 30 min and then mounting with mounting media (Vectashield). Images were acquired with Zeiss LSM 710 big confocal microscope using an x63 PL APO oil DIC On 1.4 objective for all experiments. Images were taken in Z-stacks with a voxel size of 300 nm. A Z-stack or Standard deviation intensity projections of Z-stacks are shown.

Chromatin immunoprecipitation and library preparation. Cells were cross-linked in DMEM containing 1.2 % of paraformaldehyde at RT for 10 min with rotation. Cross-link was stopped by the addition of glycine to a final concentration of 0.125M for 5 min. Cell were harvested and lysed in cell lysis buffer (10 mM Tris-HCl pH 7.4, 15 mM NaCl, 60 mM KCL, 1 mM EDTA, 0.1 mM EGTA, 0.2% NP-40, 5% sucrose). After 10 min in ice, cell lysis was amplified with a 2mL dounce (Kimble Chase) to enhance the nuclei separation from cytoplasm. Cell lysis buffer containing lysed cells was deposit up to a pillow buffer (10 mM Tris-HCl pH 7.4, 15 mM NaCl, 60 mM KCL, 1 mM EDTA, 0.1 mM EGTA, 0.2% NP-40, 10% sucrose). Nuclei were then pelleted

by centrifugation and wash with washing buffer (10 mM Tris-HCl pH 7.4, 15 mM NaCl, 60 mM KCl). Nuclei were then resuspended in sonication buffer (50 mM Tris-HCl pH 7.5, 150 mM KCl, 5 mM EDTA, 1% NP-40, 0.1% SDS, 0.5 % Sodium deoxycholate, Protease Inhibitor (Roche)). Chromatin was sheared using a Bioruptor (Diagenode) (30 cycles, 30 sec ON/ 30 sec OFF) in order to obtain chromatin fragments with an average size of 300-500 bp. Quality and size of chromatin fragments was monitored by ethidium-bromide stained agarose gel electrophoresis after DNA purification. Then, 100 µg of DNA was incubated with antibody O/N at 4°C on a rotation wheel. Antibodies are described in the S1 Table. 3 mg of protein A magnetic dynabeads (Sigma) were added for 3h at 4°C on a rotation wheel. Immunoprecipitates were then exposed to serial washes for 5 min each on a rotation wheel at 4°C in the following buffers (two times/buffer) : WB_I: 2 mM EDTA, 20 mM Tris pH 8.1, 1 % Triton 100X, 150 mM NaCl, WB_{II}: 2 mM EDTA, 20 mM Tris pH 8.1, 1 % Triton X100, 500 mM NaCl, WB_{III}: 1 mM EDTA, 10 mM Tris pH 8.1, 250 mM LiCl, 1 % Sodium deoxycholate, 1 % NP-40 and WB_{IV}: 1 M EDTA, 10 mM Tris pH 8.1. Chromatin was eluted from the magnetic beads with DNA isolation buffer (2% SDS, 0.1 M NaHCO₃) for 1h at 65°C under agitation. Extracts were reverse-crosslinked with SDS O/N at 65°C. RNAs were degraded with RNase A and proteins were finally degraded with proteinase K. Same procedure was performed for input (10 µg of DNA). DNA was finally extracted with a phenol-chloroform extraction. Quantity and quality of DNA was tested with a nanodrop (NanoDrop2000, Thermo). Samples were sequenced with the GeT core facility, Toulouse, France (<http://get.genotoul.fr>). Sequencing was done HiSeq3000-HWI-J00115 according to the manufacturer's protocol. Same procedure was done for ChIPqPCR, expected that 20 µg of DNA was used with 1µg of antibody). The sequences of the primers used are available in

Supplementary Table 7. For western blot analysis, extracts (Input (10% IP), No immunoprecipitated (NoIP) fraction and IP fraction were processed as ChIP extract but not incubated with the proteinase K and RNAase A. Extracts were then subjected to western blot analysis as previously described in the western blot paragraph. To compare different extracts, we loaded 2 % of Input, 0.5 % of Input, 0.5 % of NoIP fraction and 20% of IP fraction. Percentages are relative to the DNA quantity used for ChIP (100 µg).

ChIP-seq of H3K27ac, H3K4me1, H3K4me3, H3K36me3 and Pol II were done essentially as previously described [62]. Briefly, after cell fixation with 1 % of paraformaldehyde at RT for 5 min, cells were incubated in cell lysis buffer (PIPES 5 mM, KCL 85 mM, NP40 0.5%, Na Butyrate 10 mM, protease inhibitors) for 10 min on ice. After mild centrifugation, nuclei were lysed in Nuclei Lysis Buffer (Tris-HCL 50 mM pH 7.5, SDS 0.125%, EDTA 10 mM, Na Butyrate 10 mM, protease inhibitors) at 4°C for 2h and, then, sonicated for 10 cycles at 4°C using BioruptorPico device from Diagenode. For immunoprecipitation of H3K4me1, H3K4me3 and H3K27ac, 150 µl of chromatin (equivalent to $4 \cdot 10^6$ cells) and 4.5 µg of the corresponding antibodies were used. For Pol II, 850 µl of chromatin (equivalent to $22 \cdot 10^6$ cells) and 20 µg of the corresponding antibody were used. Two independent replicates for each ChIP were sequenced by the MGX genomic platform (Montpellier) using the Hi-seq2500 Illumina sequencer.

Strand-specific total RNA library preparation. Total RNA was isolated using the RNAeasy midi kit (Qiagen). RNA-seq quality and quantity control were performed using a Nanodrop (NanoDrop2000, Thermo) and BioAnalyser. Library preparation and sequencing was done by GeT core facility, Toulouse, France (<http://get.genotoul.fr>) with the kit TruSeq Stranded total RNA according to

manufacturer's institutions. Sequencing was done HiSeq3000-HWI-J00115 according to the manufacturer's protocol.

ChIP-seq data processing. The quality of the reads was estimated with FastQC (Illumina, 1.0.0). Published ChIP-seq data of H3K9me3 (GSM2258862), H3K27me3 (GSM2258850) and corresponding input (GSM2258864) in MDA-MB231 cells were downloaded from GEODATASETS (<https://www.ncbi.nlm.nih.gov/geo/>, GEO accession number : GSE85158) [33], and reanalyzed as subsequently described. Published ChIP-seq data of BRD4 in MDA-MB231 cells were downloaded (GSM2862187) and corresponding input (GSM2862178) from GEODATASETS (<https://www.ncbi.nlm.nih.gov/geo/>, GEO accession number : GSE107176) [63], and reanalyzed as subsequently described. Sequenced reads were aligned to the human genome Assembly GRCh38 using STAR (2.5.1) algorithm with defaults parameters[64]. Details are supplied in Supplementary Table 2. Low quality reads were then filtered out using Samtools (Samtools, options `-q 10 -view`) [65]. Conversion of BAM files to bigWig files was performed with Bamcompare tool (DeepTools utilities v3.1.3) [66]. Corresponding ChIP-seq data generated from genomic DNA (Input) were used as control for every bigWig files normalization (options: `--normalizeUsing RPKM --operation subtract --binSize 50 bp --smoothLength 150 bp`). Peaks were determined with the enrichR function of NormR package [67] (v3.8, Options: `fdr = 5e-2, binsize = 500 bp` for H3K27ac, H3K4me1, H3K4me3, BRD4 and `binsize = 3000 bp` for H3K36me3, PolII, H3K9me3, H3K27me3, Ab α H2A1.1 and Ab α H2A1). Peaks of Ab α H2A1.1 (and Ab α H2A1) spaced less than 3000 bp on the linear genome were merged. All downstream analyses were mainly performed with R studio. ChIP-seq signal and peaks positions visualization were obtained with IGV [68,69]. Boxplots were done with ggplot2 [70]. Distributions of

mH2A1 isoforms and H3K27me3/H3K9me3 common peaks identified at specific genomic features were calculated using ChIPseeker package with default parameters (Figs 1B and S5B) [71]. Statistical analyses are presented in Statistics and Reproducibility paragraph.

Identification of “putative” enhancers and super-enhancers. All putative enhancers correspond to the union of H3K4me1 and H3K27ac outside TSS (+/- 2 kb) to avoid TSS bias (Fig 2B) [72]. TSS annotation is based on TxDb.Hsapiens.UCSC.hg38.knownGene release. Super-enhancers were determined with ROSE utility tools based on H3K27ac signal (options : stitching_distance = 12.5 kb and TSS_exclusion_zone_size : 2500 bp) (Fig 2C and 2D) [36,37].

Pol II pausing index calculation. Pausing index (PI) was defined as previously[73], which is the ratio of Pol II (total) density in the promoter-proximal region ([-30;300] bp centered on TSS) to the total Pol II density in the transcribed regions (TSS + 300 bp to TES). Pausing index was only calculated for actively expressed genes (n=10,198, see RNA-seq analysis). Paused genes were defined as genes that have a PI upper to 2 (n=6,821).

Venn diagrams. Intersection of peaks were determined with the function findOverlaps() from GenomicRanges package. To note that for two ChIP-seq peaks intersections, only number of overlaps is contabilised and not the number of each peaks contained per overlap. This particularity explained why number of peaks changes between venn diagrams for a same ChIP-seq (i.e Fig 1A Ab α H2A1.1 (n=29,112) and Fig 1C α H2A1.1 (n=19,867)). The area-proportional Venn diagrams were drawn based on images generated by Vennrable package. For Venn diagrams in Fig 3, 5 and S6, intersections were performed at TSS (1-bp or +/- 1kb centered on

TSS). Enrichment tests associated to Venn diagrams are explained in Statistics and Reproducibility paragraph.

Correlation heatmaps. Correlation heatmaps were done with multiBigwigSummary (options: -bins for whole genome (S2A Fig) or -BED-file for Heterochromatin, enhancer, TSS +/-1kp; TSS 1-bp, Figs S2B, S6A and S7B) and plotCorrelation (option: -spearman correlation heatmap) from DeepTools utilities (3.1.3) [66].

Metagenes profils. Metagene analysis profiles were performed with R Seqplot package using bigWig files (function getPlotSetArray and plotAverage) [74]. Heatmaps profiles of Pol II, Ab α mH2A1.1 and Ab α mH2A1 around TSS +/- 10 kb were ranked by mH2A1.1 KD de-regulated genes (mH2A1.1-activated and repressed genes, not ranked by the deregulation level) and done with Seqplot package (function getPlotSetArray and plotHeatmap) (Fig 4B). Heatmaps profiles of Pol II, Ab α mH2A1.1 and Ab α mH2A1 around TSS +/- 10 kb were ranked by pausing index and carried out with Seqplot package (function getPlotSetArray and plotHeatmap)(Fig 5A).

RNA-seq analysis. The quality of the reads was estimated with FastQC (Illumina, 1.0.0). The reads were mapped to the human reference genome GRCh38 using the default parameters of STAR (2.5.1) [64]. Details are supplied in S1 Table . Low quality reads and duplicates were then filtered out using SAMtools (Samtools, options -q 10 -view ; -rmdup)[65]. Unstranded normalized Bedgraph files in Read Per Millions (RPM) were obtained with STAR using Output Wiggle parameters (options : -outWigTypebedgraph; --outWigStrandUnstranded; --outWigNorm RPM) [64]. Gene counts were performed with htseq-count utilities with default parameters (0.8.0) [74]. FPKM for all genes were calculated with the formula : $FPKM = (RC_g \times 10^6) / (RC_p \times L)$ where RC_g corresponds to the number of reads mapped to the gene, RC_p to the

number of reads mapped to all protein-coding genes and L, the Length of the gene in base pairs. Differential expression analysis was performed with DESeq2 package [75] with cutoff $|FC| > 1.5$ and $padj < 0.1$. Corresponding volcano plot was done with EnhancedVolcano package [76] (Fig 4A). The mH2A1.1 KD de-regulated genes are listed in S3 Table.

GO analysis. GO analysis was performed with LIMMA package (--function goana) (3.8)[77] and corresponding GO terms are supplied in the S4 Table. Selection of genes related to their functions was done with biomaRt package (function getBM()) [78,79]. We took genes related to: cytoskeleton (GO:0005856), cell adhesion (GO:0007155), Cilium (GO:0005929) and cell junction (GO:0030054) (n=6,821).

Transwell migration assay. Transwell migration assays were performed using Transwell plates with 0.8 μ m pore polycarbonate membranes (CorningTranswell, Sigma). Three days post siRNA transfection, MDA-MB231 cells (10^5) were seeded in the upper chamber without FBS and allowed to invade to the reverse side of the chamber under chemoattractant condition with 10% FBS medium in the lower chamber. Following incubation for 16h at 37°C, the cells were fixed with 3.7% formaldehyde for 2 min at RT. Cells permeabilization was carried out with methanol incubation for 20 min at RT. Cells were then stained with Giesma for 15 min at RT. Same final total cell number between conditions was always checked by wide field microscope to avoid proliferation bias during number of migratory cell comparison. Not migrated cells were finally removed from the upper chamber by using a cotton swab. Migrated cells adhering to the underside of the chamber were photographed using a light microscope at x200 magnification (Invitrogen EVOS Digital Color Fluorescence Microscope). Cell counting was done with ImageJ in ten different fields

per condition[80]. Three independent experiments were performed for each condition.

Statistics and reproducibility. All western blot, RTqPCR and Boyden Chamber assay experiments were repeated at least twice as independent biological replicates and results are presented as mean +/- sd. All statistical analyses were done with R. For Western blot, RTqPCR and Boyden Chamber, Wilcoxon tests were used to compare mean values between conditions. p-values were considered as significant when $* \leq 0.05$ and highly significant when $** \leq 0.01$; $*** \leq 0.001$; $**** \leq 0.0001$. All enrichment tests were performed on a base set made up of genomic bins. Each genomic bin is defined by merging ranges of ChIP-seq data (reduce function GenomicRanges R package) ChIP-seq list : Ab α mH2A1.1, Ab α mH2A1, Pol II, H3K4me3, H3K4me1, H3K36me3, H3K27ac, H3K27me3, H3K9me3, “putative” enhancers and “putative” Super-enhancers, on whole genome or TSS +/- 1kb and TSS 1-bp.

Data availability. ChIP-seq and RNA-seq data have been deposited to GEO under accession number GSE140022. Additional data are available upon reasonable request.

Acknowledgements

We thank M. Buschbeck from JCLR Institute at Barcelona for kindly providing Flag-mH2A1.1 and Flag-mH2A1.2 expression plasmids. ChIP-seq data against mH2A1.1 and mH2A1 isoforms as well as RNA-seq data were performed in collaboration with the GeT core facility, Toulouse, France (<http://get.genotoul.fr>), and were supported by France Génomique National infrastructure, funded as part of “Investissement

d’avenir” program managed by Agence Nationale pour la Recherche (contract ANR-10-INBS-09) and by the Fondation Recherche Medical (DEQ43940 to O.C team including A.H). We thank Marc Piechaszky for critical reading of the manuscript. We acknowledge support from the light imaging Toulouse CBI platform. The work was generously funded by the Institut National du Cancer (INCA PL-BIO-16-269) to KB.

Author contributions

L.R, A-C.L and K.B conceived this study. F.M validated custom Ab α mH2A1.1 antibody specificity against mH2A1.1. L.R performed ChIP-seq against mH2A1 isoforms and RNA-seq. I.E-J. and F.B performed ChIP-seq against active histone marks. L.R, A.H and F.R realized bioinformatic analysis of all ChIP-seq and RNA-seq data. Statistical analyses were done by A.H and L.R. L.R performed all other experimental data. L.R, A-C.L and K.B designed experiments and interpreted results. L.R, A-C.L and K.B wrote the manuscript with input from all other authors.

Competing interests

The authors declare no competing interests.

References

1. Venkatesh S, Workman JL. Histone exchange, chromatin structure and the regulation of transcription. Nat Rev Mol Cell Biol [Internet]. 2015 Mar 4 [cited 2019 Nov 6];16(3):178–89. Available from: <http://www.ncbi.nlm.nih.gov/pubmed/25650798>
2. Luger K, Dechassa ML, Tremethick DJ. New insights into nucleosome and

- chromatin structure: an ordered state or a disordered affair? *Nat Rev Mol Cell Biol* [Internet]. 2012 Jul 22 [cited 2019 Jul 23];13(7):436–47. Available from: <http://www.ncbi.nlm.nih.gov/pubmed/22722606>
3. Buschbeck M, Hake SB. Variants of core histones and their roles in cell fate decisions, development and cancer. *Nat Rev Mol Cell Biol* [Internet]. 2017 Feb 1 [cited 2017 May 10];18(5):299–314. Available from: <http://www.ncbi.nlm.nih.gov/pubmed/28144029>
4. Pehrson JR, Fuji RN. Evolutionary conservation of histone macroH2A subtypes and domains. *Nucleic Acids Res* [Internet]. 1998 Jun 15 [cited 2019 Jul 23];26(12):2837–42. Available from: <https://academic.oup.com/nar/article-lookup/doi/10.1093/nar/26.12.2837>
5. Rivera-Casas C, Gonzalez-Romero R, Cheema MS, Ausió J, Eirín-López JM. The characterization of macroH2A beyond vertebrates supports an ancestral origin and conserved role for histone variants in chromatin. *Epigenetics* [Internet]. 2016 Jun 2 [cited 2019 Jul 23];11(6):415–25. Available from: <http://www.tandfonline.com/doi/full/10.1080/15592294.2016.1172161>
6. Gamble MJ, Kraus WL. Multiple facets of the unique histone variant macroH2A: From genomics to cell biology. *Cell Cycle*. 2010;9(13):2568–74.
7. Costanzi C, Pehrson JR. Histone macroH2A1 is concentrated in the inactive X chromosome of female mammals. *Nature*. 1998;628(1997):1997–9.
8. Gamble MJ, Frizzell KM, Yang C, Krishnakumar R, Kraus WL. The histone variant macroH2A1 marks repressed autosomal chromatin, but protects a subset of its target genes from silencing. *Genes Dev* [Internet]. 2010 Jan 1 [cited 2019 Jul 23];24(1):21–32. Available from: <http://genesdev.cshlp.org/cgi/doi/10.1101/gad.1876110>

9. Douet J, Corujo D, Malinverni R, Renauld J, Sansoni V, Posavec Marjanović M, et al. MacroH2A histone variants maintain nuclear organization and heterochromatin architecture. *J Cell Sci.* 2017;130(9):1570–82.
10. Sun Z, Filipescu D, Andrade J, Gaspar-Maia A, Ueberheide B, Bernstein E. Transcription-associated histone pruning demarcates macroH2A chromatin domains. *Nat Struct Mol Biol [Internet].* 2018 Oct 5 [cited 2019 Jul 23];25(10):958–70. Available from: <http://www.nature.com/articles/s41594-018-0134-5>
11. Doyen C-M, An W, Angelov D, Bondarenko V, Mietton F, Studitsky VM, et al. Mechanism of polymerase II transcription repression by the histone variant macroH2A. *Mol Cell Biol [Internet].* 2006 Feb 1 [cited 2019 Jul 23];26(3):1156–64. Available from: <http://mcb.asm.org/cgi/doi/10.1128/MCB.26.3.1156-1164.2006>
12. Angelov D, Molla A, Perche P-Y, Hans F, Côté J, Khochbin S, et al. The histone variant macroH2A interferes with transcription factor binding and SWI/SNF nucleosome remodeling. *Mol Cell [Internet].* 2003 Apr [cited 2019 Jul 23];11(4):1033–41. Available from: <http://www.ncbi.nlm.nih.gov/pubmed/12718888>
13. Dell'Orso S, Wang AH, Shih H-Y, Saso K, Berghella L, Gutierrez-Cruz G, et al. The Histone Variant MacroH2A1.2 Is Necessary for the Activation of Muscle Enhancers and Recruitment of the Transcription Factor Pbx1. *Cell Rep [Internet].* 2016 Feb 9 [cited 2019 Jul 23];14(5):1156–68. Available from: <https://linkinghub.elsevier.com/retrieve/pii/S2211124716000036>
14. Chen H, Ruiz PD, Novikov L, Casill AD, Park JW, Gamble MJ. MacroH2A1.1 and PARP-1 cooperate to regulate transcription by promoting CBP-mediated

- 789 H2B acetylation. *Nat Struct Mol Biol* [Internet]. 2014 Oct 12 [cited 2016 Nov
790 19];21(11):981–9. Available from:
791 <http://www.nature.com/doi/10.1038/nsmb.2903>
- 792 15. Podrini C, Koffas A, Chokshi S, Vinciguerra M, Lelliott CJ, White JK, et al.
793 MacroH2A1 isoforms are associated with epigenetic markers for activation of
794 lipogenic genes in fat-induced steatosis. *FASEB J* [Internet]. 2015 May [cited
795 2019 Jul 23];29(5):1676–87. Available from:
796 <http://www.fasebj.org/doi/10.1096/fj.14-262717>
- 797 16. Wan D, Liu C, Sun Y, Wang W, Huang K, Zheng L. MacroH2A1.1 cooperates
798 with EZH2 to promote adipogenesis by regulating Wnt signaling. *J Mol Cell Biol*
799 [Internet]. 2017 Aug 1 [cited 2019 Jul 23];9(4):325–37. Available from:
800 [http://academic.oup.com/jmcb/article/9/4/325/4067698/MacroH2A11-](http://academic.oup.com/jmcb/article/9/4/325/4067698/MacroH2A11-cooperates-with-EZH2-to-promote)
801 [cooperates-with-EZH2-to-promote](http://academic.oup.com/jmcb/article/9/4/325/4067698/MacroH2A11-cooperates-with-EZH2-to-promote)
- 802 17. Changoikar LN, Singh G, Cui K, Berletch JB, Zhao K, Disteché CM, et al.
803 Genome-wide distribution of macroH2A1 histone variants in mouse liver
804 chromatin. *Mol Cell Biol* [Internet]. 2010 Dec 1 [cited 2019 Jul 23];30(23):5473–
805 83. Available from: <http://mcb.asm.org/cgi/doi/10.1128/MCB.00518-10>
- 806 18. Posavec Marjanović M, Hurtado-Bagès S, Lassi M, Valero V, Malinverni R,
807 Delage H, et al. MacroH2A1.1 regulates mitochondrial respiration by limiting
808 nuclear NAD⁺ consumption. *Nat Struct Mol Biol* [Internet]. 2017 Nov 9 [cited
809 2019 Aug 7];24(11):902–10. Available from:
810 <http://www.nature.com/articles/nsmb.3481>
- 811 19. Sporn JC, Kustatscher G, Hothorn T, Collado M, Serrano M, Muley T, et al.
812 Histone macroH2A isoforms predict the risk of lung cancer recurrence.
813 *Oncogene* [Internet]. 2009 Sep 3 [cited 2019 Jul 23];28(38):3423–8. Available

from: <http://www.ncbi.nlm.nih.gov/pubmed/19648962>

20. Cantariño N, Douet J, Buschbeck M. MacroH2A – An epigenetic regulator of cancer. *Cancer Lett* [Internet]. 2013 Aug [cited 2019 Jul 23];336(2):247–52. Available from: <https://linkinghub.elsevier.com/retrieve/pii/S0304383513002504>
21. Sporn JC, Jung B. Differential regulation and predictive potential of MacroH2A1 isoforms in colon cancer. *Am J Pathol* [Internet]. 2012 Jun [cited 2019 Jul 23];180(6):2516–26. Available from: <http://www.ncbi.nlm.nih.gov/pubmed/22542848>
22. Mermoud JE, Costanzi C, Pehrson JR, Brockdorff N. Histone MacroH2A1 . 2 Relocates to the Inactive X Chromosome after Initiation and Propagation of X-Inactivation. *J Cell Biol*. 1999;147(7):1399–408.
23. Pliatska M, Kapasa M, Kokkalis A, Polyzos A, Thanos D. The Histone Variant MacroH2A Blocks Cellular Reprogramming by Inhibiting Mesenchymal-to-Epithelial Transition. *Mol Cell Biol* [Internet]. 2018 Feb 15 [cited 2019 Jul 23];38(10):e00669-17. Available from: <http://mcb.asm.org/lookup/doi/10.1128/MCB.00669-17>
24. Lavigne A-C, Castells M, Mermet J, Kocanova S, Dalvai M, Bystricky K. Increased macroH2A1.1 expression correlates with poor survival of triple-negative breast cancer patients. Haibe-Kains B, editor. *PLoS One* [Internet]. 2014 Jun 9 [cited 2019 Jul 23];9(6):e98930. Available from: <https://dx.plos.org/10.1371/journal.pone.0098930>
25. Kustatscher G, Hothorn M, Pugieux C, Scheffzek K, Ladurner AG. Splicing regulates NAD metabolite binding to histone macroH2A. *Nat Struct Mol Biol* [Internet]. 2005 Jul 19 [cited 2019 Jul 23];12(7):624–5. Available from: <http://www.ncbi.nlm.nih.gov/pubmed/15965484>

26. Ray Chaudhuri A, Nussenzweig A. The multifaceted roles of PARP1 in DNA repair and chromatin remodelling. *Nat Rev Mol Cell Biol* [Internet]. 2017 Oct 5 [cited 2019 Jul 23];18(10):610–21. Available from: <http://www.ncbi.nlm.nih.gov/pubmed/28676700>
27. Ouarrhni K, Hadj-Slimane R, Ait-Si-Ali S, Robin P, Mietton F, Harel-Bellan A, et al. The histone variant mH2A1.1 interferes with transcription by down-regulating PARP-1 enzymatic activity. *Genes Dev* [Internet]. 2006 Dec 1 [cited 2019 Jul 23];20(23):3324–36. Available from: <http://www.genesdev.org/cgi/doi/10.1101/gad.396106>
28. Marjanović MP, Hurtado-bagès S, Lassi M, Valero V, Malinverni R, Delage H, et al. MacroH2A1 . 1 regulates mitochondrial respiration by limiting nuclear NAD + consumption. 2018;24(11):902–10.
29. Xu C, Xu Y, Gursoy-Yuzugullu O, Price BD. The histone variant macroH2A1.1 is recruited to DSBs through a mechanism involving PARP1. *FEBS Lett* [Internet]. 2012 Nov 2 [cited 2019 Jul 23];586(21):3920–5. Available from: <http://doi.wiley.com/10.1016/j.febslet.2012.09.030>
30. Kim J, Oberdoerffer P, Khurana S. The histone variant macroH2A1 is a splicing-modulated caretaker of genome integrity and tumor growth. *Mol Cell Oncol* [Internet]. 2018 Mar 7 [cited 2019 Jul 23];5(3):e1441629. Available from: <https://www.tandfonline.com/doi/full/10.1080/23723556.2018.1441629>
31. Chen H, Ruiz PD, McKimpson WM, Novikov L, Kitsis RN, Gamble MJ. MacroH2A1 and ATM Play Opposing Roles in Paracrine Senescence and the Senescence-Associated Secretory Phenotype. *Mol Cell* [Internet]. 2015 Sep [cited 2019 Dec 11];59(5):719–31. Available from: <https://linkinghub.elsevier.com/retrieve/pii/S1097276515005699>

32. Ouarrhni K, Hadj-Slimane R, Ait-Si-Ali S, Robin P, Muetton F, Harel-Bellan A, et al. The histone variant mH2A1.1 interferes with transcription by down-regulating PARP-1 enzymatic activity. *Genes Dev* [Internet]. 2006 Dec 1 [cited 2019 Dec 11];20(23):3324–36. Available from: <http://www.genesdev.org/cgi/doi/10.1101/gad.396106>
33. Franco HL, Nagari A, Malladi VS, Li W, Xi Y, Richardson D, et al. Enhancer transcription reveals subtype-specific gene expression programs controlling breast cancer pathogenesis. *Genome Res* [Internet]. 2018 Feb [cited 2019 Jul 23];28(2):159–70. Available from: <http://genome.cshlp.org/lookup/doi/10.1101/gr.226019.117>
34. Allshire RC, Madhani HD. Ten principles of heterochromatin formation and function. *Nat Rev Mol Cell Biol* [Internet]. 2018 Apr 13 [cited 2019 Jul 26];19(4):229–44. Available from: <http://www.nature.com/articles/nrm.2017.119>
35. Creighton MP, Cheng AW, Welstead GG, Kooistra T, Carey BW, Steine EJ, et al. Histone H3K27ac separates active from poised enhancers and predicts developmental state. *Proc Natl Acad Sci* [Internet]. 2010 Dec 14 [cited 2019 Jul 23];107(50):21931–6. Available from: <http://www.pnas.org/cgi/doi/10.1073/pnas.1016071107>
36. Whyte WA, Orlando DA, Hnisz D, Abraham BJ, Lin CY, Kagey MH, et al. Master Transcription Factors and Mediator Establish Super-Enhancers at Key Cell Identity Genes. *Cell* [Internet]. 2013 Apr [cited 2019 Jul 23];153(2):307–19. Available from: <https://linkinghub.elsevier.com/retrieve/pii/S0092867413003929>
37. Lovén J, Hoke HA, Lin CY, Lau A, Orlando DA, Vakoc CR, et al. Selective inhibition of tumor oncogenes by disruption of super-enhancers. *Cell* [Internet]. 2013 Apr 11 [cited 2019 Jul 23];153(2):320–34. Available from:

<https://linkinghub.elsevier.com/retrieve/pii/S0092867413003930>

38. Adelman K, Lis JT. Promoter-proximal pausing of RNA polymerase II: emerging roles in metazoans. *Nat Rev Genet* [Internet]. 2012 Oct 18 [cited 2019 Jul 23];13(10):720–31. Available from: <http://www.ncbi.nlm.nih.gov/pubmed/22986266>
39. Novikov L, Park JW, Chen H, Klerman H, Jalloh AS, Gamble MJ. QKI-mediated alternative splicing of the histone variant MacroH2A1 regulates cancer cell proliferation. *Mol Cell Biol* [Internet]. 2011 Oct 15 [cited 2019 Jul 23];31(20):4244–55. Available from: <http://mcb.asm.org/cgi/doi/10.1128/MCB.05244-11>
40. Draheim KM, Chen H-B, Tao Q, Moore N, Roche M, Lyle S. ARRDC3 suppresses breast cancer progression by negatively regulating integrin beta4. *Oncogene* [Internet]. 2010 Sep 9 [cited 2019 Jul 23];29(36):5032–47. Available from: <http://www.nature.com/articles/onc2010250>
41. Mei Z, Chen S, Chen C, Xiao B, Li F, Wang Y, et al. Interleukin-23 Facilitates Thyroid Cancer Cell Migration and Invasion by Inhibiting SOCS4 Expression via MicroRNA-25. Zhang Z, editor. *PLoS One* [Internet]. 2015 Oct 5 [cited 2019 Jul 23];10(10):e0139456. Available from: <https://dx.plos.org/10.1371/journal.pone.0139456>
42. Castillo-Lluva S, Tan C-T, Daugaard M, Sorensen PHB, Malliri A. The tumour suppressor HACE1 controls cell migration by regulating Rac1 degradation. *Oncogene* [Internet]. 2013 Mar 28 [cited 2019 Jul 23];32(13):1735–42. Available from: <http://www.nature.com/articles/onc2012189>
43. Stankiewicz E, Mao X, Mangham DC, Xu L, Yeste-Velasco M, Fisher G, et al. Identification of FBXL4 as a Metastasis Associated Gene in Prostate Cancer.

- 914 Sci Rep [Internet]. 2017 Dec 11 [cited 2019 Jul 23];7(1):5124. Available from:
915 <http://www.nature.com/articles/s41598-017-05209-z>
- 916 44. Pinzaglia M, Montaldo C, Polinari D, Simone M, La Teana A, Tripodi M, et al.
917 EIF6 over-expression increases the motility and invasiveness of cancer cells by
918 modulating the expression of a critical subset of membrane-bound proteins.
919 BMC Cancer [Internet]. 2015 Mar 15 [cited 2019 Jul 23];15(1):131. Available
920 from: <http://bmccancer.biomedcentral.com/articles/10.1186/s12885-015-1106-3>
- 921 45. Ryu H-H, Jung S, Jung T-Y, Moon K-S, Kim I-Y, Jeong Y-I, et al. Role of
922 metallothionein 1E in the migration and invasion of human glioma cell lines. Int
923 J Oncol [Internet]. 2012 Oct [cited 2019 Jul 23];41(4):1305–13. Available from:
924 <https://www.spandidos-publications.com/10.3892/ijo.2012.1570>
- 925 46. Selvaraj N, Budka JA, Ferris MW, Plotnik JP, Hollenhorst PC. Extracellular
926 signal-regulated kinase signaling regulates the opposing roles of JUN family
927 transcription factors at ETS/AP-1 sites and in cell migration. Mol Cell Biol
928 [Internet]. 2015 Jan 1 [cited 2019 Jul 23];35(1):88–100. Available from:
929 <http://mcb.asm.org/lookup/doi/10.1128/MCB.00982-14>
- 930 47. Kake S, Usui T, Ohama T, Yamawaki H, Sato K. Death-associated protein
931 kinase 3 controls the tumor progression of A549 cells through ERK MAPK/c-
932 Myc signaling. Oncol Rep [Internet]. 2017 Feb [cited 2019 Jul 23];37(2):1100–
933 6. Available from: [https://www.spandidos-](https://www.spandidos-publications.com/10.3892/or.2017.5359)
934 [publications.com/10.3892/or.2017.5359](https://www.spandidos-publications.com/10.3892/or.2017.5359)
- 935 48. Lavigne MD, Vatsellas G, Polyzos A, Mantouvalou E, Sianidis G, Maraziotis I,
936 et al. Composite macroH2A/NRF-1 Nucleosomes Suppress Noise and
937 Generate Robustness in Gene Expression. Cell Rep [Internet]. 2015 May [cited
938 2019 Jul 23];11(7):1090–101. Available from:

<https://linkinghub.elsevier.com/retrieve/pii/S221112471500409X>

49. Segal T, Salmon-Divon M, Gerlitz G. The Heterochromatin Landscape in Migrating Cells and the Importance of H3K27me3 for Associated Transcriptome Alterations. *Cells* [Internet]. 2018 Nov 9 [cited 2019 Jul 23];7(11):205. Available from: <http://www.mdpi.com/2073-4409/7/11/205>
50. Yokoyama Y, Hieda M, Nishioka Y, Matsumoto A, Higashi S, Kimura H, et al. Cancer-associated upregulation of histone H3 lysine 9 trimethylation promotes cell motility in vitro and drives tumor formation in vivo. *Cancer Sci* [Internet]. 2013 Jul [cited 2019 Aug 7];104(7):889–95. Available from: <http://doi.wiley.com/10.1111/cas.12166>
51. Bernstein E, Muratore-Schroeder TL, Diaz RL, Chow JC, Changolkar LN, Shabanowitz J, et al. A phosphorylated subpopulation of the histone variant macroH2A1 is excluded from the inactive X chromosome and enriched during mitosis. *Proc Natl Acad Sci U S A* [Internet]. 2008 Feb 5 [cited 2019 Jul 23];105(5):1533–8. Available from: <http://www.pnas.org/cgi/doi/10.1073/pnas.0711632105>
52. Dardenne E, Pierredon S, Driouch K, Gratadou L, Lacroix-Triki M, Espinoza MP, et al. Splicing switch of an epigenetic regulator by RNA helicases promotes tumor-cell invasiveness. *Nat Struct Mol Biol* [Internet]. 2012 Nov 30 [cited 2019 Jul 23];19(11):1139–46. Available from: <http://www.nature.com/articles/nsmb.2390>
53. Kapoor A, Goldberg MS, Cumberland LK, Ratnakumar K, Segura MF, Emanuel PO, et al. The histone variant macroH2A suppresses melanoma progression through regulation of CDK8. 2011;468(7327):1105–9.
54. Borghesan M, Fusilli C, Rappa F, Panebianco C, Rizzo G, Oben JA, et al. DNA

- Hypomethylation and Histone Variant macroH2A1 Synergistically Attenuate
Chemotherapy-Induced Senescence to Promote Hepatocellular Carcinoma
Progression. 2017;76(3):594–606.
55. Li F, Yi P, Pi J, Li L, Hui J, Wang F, et al. QKI5-mediated alternative splicing of
the histone variant macroH2A1 regulates gastric carcinogenesis. Oncotarget
[Internet]. 2016 May 31 [cited 2019 Jul 23];7(22):32821–34. Available from:
<http://www.oncotarget.com/fulltext/8739>
56. Gibson BA, Zhang Y, Jiang H, Hussey KM, Shrimp JH, Lin H, et al. Chemical
genetic discovery of PARP targets reveals a role for PARP-1 in transcription
elongation. Science (80-) [Internet]. 2016 Jul 1 [cited 2019 Aug
7];353(6294):45–50. Available from:
<http://www.ncbi.nlm.nih.gov/pubmed/27256882>
57. Hnisz D, Abraham BJ, Lee TI, Lau A, Saint-André V, Sigova AA, et al. Super-
Enhancers in the Control of Cell Identity and Disease. Cell [Internet]. 2013 Nov
7 [cited 2019 Aug 6];155(4):934–47. Available from:
<http://www.ncbi.nlm.nih.gov/pubmed/24119843>
58. Donati B, Lorenzini E, Ciarrocchi A. BRD4 and Cancer: going beyond
transcriptional regulation. Mol Cancer [Internet]. 2018 Dec 22 [cited 2019 Aug
6];17(1):164. Available from: [https://molecular-](https://molecular-cancer.biomedcentral.com/articles/10.1186/s12943-018-0915-9)
[cancer.biomedcentral.com/articles/10.1186/s12943-018-0915-9](https://molecular-cancer.biomedcentral.com/articles/10.1186/s12943-018-0915-9)
59. He Y, Long W, Liu Q. Targeting Super-Enhancers as a Therapeutic Strategy
for Cancer Treatment. Front Pharmacol [Internet]. 2019 Apr 11 [cited 2019 Aug
6];10:361. Available from: <http://www.ncbi.nlm.nih.gov/pubmed/31105558>
60. Yang P-C, Liu Z-Q, Mahmood T. Western blot: Technique, theory and trouble
shooting. N Am J Med Sci [Internet]. 2014 [cited 2019 Jul 23];6(3):160.

- 989 Available from: <http://www.najms.org/text.asp?2014/6/3/160/128482>
- 990 61. Rao X, Huang X, Zhou Z, Lin X. An improvement of the 2⁻(-delta delta CT)
- 991 method for quantitative real-time polymerase chain reaction data analysis.
- 992 Biostat Bioinforma Biomath [Internet]. 2013 Aug [cited 2019 Jul 23];3(3):71–85.
- 993 Available from: <http://www.ncbi.nlm.nih.gov/pubmed/25558171>
- 994 62. Tolza C, Bejjani F, Evanno E, Mahfoud S, Moquet-Torcy G, Gostan T, et al.
- 995 AP-1 Signaling by Fra-1 Directly Regulates HMGA1 Oncogene Transcription in
- 996 Triple-Negative Breast Cancers. Mol Cancer Res [Internet]. 2019 Oct [cited
- 997 2019 Oct 29];17(10):1999–2014. Available from:
- 998 <http://mcr.aacrjournals.org/lookup/doi/10.1158/1541-7786.MCR-19-0036>
- 999 63. Chan HL, Beckedorff F, Zhang Y, Garcia-Huidobro J, Jiang H, Colaprico A, et
- 1000 al. Polycomb complexes associate with enhancers and promote oncogenic
- 1001 transcriptional programs in cancer through multiple mechanisms. Nat Commun
- 1002 [Internet]. 2018 [cited 2019 Aug 7];9(1):3377. Available from:
- 1003 <http://www.ncbi.nlm.nih.gov/pubmed/30139998>
- 1004 64. Dobin A, Davis CA, Schlesinger F, Drenkow J, Zaleski C, Jha S, et al. STAR:
- 1005 ultrafast universal RNA-seq aligner. Bioinformatics [Internet]. 2013 Jan 1 [cited
- 1006 2019 Jul 23];29(1):15–21. Available from:
- 1007 [https://academic.oup.com/bioinformatics/article-](https://academic.oup.com/bioinformatics/article-lookup/doi/10.1093/bioinformatics/bts635)
- 1008 [lookup/doi/10.1093/bioinformatics/bts635](https://academic.oup.com/bioinformatics/article-lookup/doi/10.1093/bioinformatics/bts635)
- 1009 65. Li H, Handsaker B, Wysoker A, Fennell T, Ruan J, Homer N, et al. The
- 1010 Sequence Alignment/Map format and SAMtools. Bioinformatics [Internet]. 2009
- 1011 Aug 15 [cited 2019 Jul 23];25(16):2078–9. Available from:
- 1012 <http://www.ncbi.nlm.nih.gov/pubmed/19505943>
- 1013 66. Ram F, Ryan DP, Bhardwaj V, Kilpert F, Richter AS, Heyne S, et al.

1014 deepTools2 : a next generation web server for deep-sequencing data analysis.
 1015 2016;44(April):160–5.

1016 67. Helmuth J CH. normr: Normalization and difference calling in ChIP-seq data . R
 1017 Packag version 180, <https://github.com/your-highness/normR>. 2018;2018.

1018 68. James T. Robinson, Helga Thorvaldsdóttir, Wendy Winckler, Mitchell Guttman,
 1019 Eric S. Lander, Gad Getz JPM. Integrative genomics viewer. Nat Biotechnol.
 1020 2000;29(220):23–4.

1021 69. Thorvaldsdóttir H, Robinson JT, Mesirov JP. Integrative Genomics Viewer
 1022 (IGV): high-performance genomics data visualization and exploration. Brief
 1023 Bioinform [Internet]. 2013 Mar 1 [cited 2019 Jul 23];14(2):178–92. Available
 1024 from: <https://academic.oup.com/bib/article-lookup/doi/10.1093/bib/bbs017>

1025 70. H. Wickham. ggplot2: Elegant Graphics for Data Analysis. Springer-Verlag
 1026 New York [Internet]. 2016;174(1):245–6. Available from:
 1027 http://doi.wiley.com/10.1111/j.1467-985X.2010.00676_9.x

1028 71. Yu G, Wang L-G, He Q-Y. ChIPseeker: an R/Bioconductor package for ChIP
 1029 peak annotation, comparison and visualization. Bioinformatics [Internet]. 2015
 1030 Jul 15 [cited 2019 Jul 23];31(14):2382–3. Available from:
 1031 [https://academic.oup.com/bioinformatics/article-](https://academic.oup.com/bioinformatics/article-lookup/doi/10.1093/bioinformatics/btv145)
 1032 [lookup/doi/10.1093/bioinformatics/btv145](https://academic.oup.com/bioinformatics/article-lookup/doi/10.1093/bioinformatics/btv145)

1033 72. Blinka S, Reimer MH, Pulakanti K, Pinello L, Yuan G-C, Rao S. Identification of
 1034 Transcribed Enhancers by Genome-Wide Chromatin Immunoprecipitation
 1035 Sequencing. Methods Mol Biol [Internet]. 2017 [cited 2019 Jul 23];1468:91–
 1036 109. Available from: <http://www.ncbi.nlm.nih.gov/pubmed/27662872>

1037 73. Zhang X, Chiang H-C, Wang Y, Zhang C, Smith S, Zhao X, et al. Attenuation of
 1038 RNA polymerase II pausing mitigates BRCA1-associated R-loop accumulation

- and tumorigenesis. Nat Commun [Internet]. 2017 Aug 26 [cited 2019 Jul 23];8(1):15908. Available from: <http://www.ncbi.nlm.nih.gov/pubmed/28649985>
74. Stempor P, Ahringer J. SeqPlots - Interactive software for exploratory data analyses, pattern discovery and visualization in genomics. Wellcome Open Res [Internet]. 2016;1(0):14. Available from: <https://wellcomeopenresearch.org/articles/1-14/v1>
75. Love MI, Huber W, Anders S. Moderated estimation of fold change and dispersion for RNA-seq data with DESeq2. Genome Biol [Internet]. 2014 Dec 5 [cited 2019 Jul 23];15(12):550. Available from: <http://genomebiology.biomedcentral.com/articles/10.1186/s13059-014-0550-8>
76. K B. EnhancedVolcano: Publication-ready volcano plots with enhanced colouring and labeling . <https://github.com/kevinblighe/EnhancedVolcano> [Internet]. 2018;R package:2018. Available from: <https://github.com/kevinblighe/EnhancedVolcano>.
77. Ritchie ME, Phipson B, Wu D, Hu Y, Law CW, Shi W, et al. Limma powers differential expression analyses for RNA-sequencing and microarray studies. Nucleic Acids Res. 2015;43(7):e47.
78. Durinck S, Moreau Y, Kasprzyk A, Davis S, De Moor B, Brazma A, et al. BioMart and Bioconductor: a powerful link between biological databases and microarray data analysis. Bioinformatics [Internet]. 2005 Aug 15 [cited 2019 Jul 23];21(16):3439–40. Available from: <https://academic.oup.com/bioinformatics/article-lookup/doi/10.1093/bioinformatics/bti525>
79. Durinck S, Spellman PT, Birney E, Huber W. Mapping identifiers for the integration of genomic datasets with the R/Bioconductor package biomaRt. Nat

Protoc [Internet]. 2009 Aug 23 [cited 2019 Jul 23];4(8):1184–91. Available from: <http://www.nature.com/articles/nprot.2009.97>

80. Caroline A Schneider WSR& KWE. NIH Image to ImageJ: 25 years of image analysis. INMATEH - Agric Eng [Internet]. 2012;9(7):671–5. Available from: <http://dx.doi.org/10.1038/nmeth.2089>

Figure legends

Fig 1. Histone mH2A1 isoforms are incorporated to “facultative-like” heterochromatin. (A) Overlap of “mH2A1.1” (Ab α mH2A1.1) peaks with “mH2A1” (Ab α mH2A1). Peaks detected exclusively by Ab α mH2A1.1 are called “mH2A1.1 only”, peaks detected exclusively by Ab α mH2A1 are called “mH2A1.2 only” and peaks detected by both correspond to mH2A1.1 only or mH2A1.1 and mH2A1.2 in unknown proportions, called “mH2A1s”. (B) Proportions of mH2A1 isoforms peaks at different genomic features (Methods). Arrows highlights differences between the two ChIP-seq. Promoters are defined around TSS. (C) Overlap of heterochromatin histone marks (H3K27me3 and H3K9me3) with mH2A1.1 peaks (left) and mH2A1 peaks (right). Percentages of overlaps are also given. Results of fisher exact tests are shown (p-value (p) and Odd ratio) (Methods). (D) Genome browser view of ChIP-seq profiles illustrating occupancy of mH2A1 isoforms with heterochromatin histone marks (H3K27me3 and H3K9me3). At the top, region with high level of H3K27me3 and at the bottom, region with high level of H3K9me3. Peaks and unstranded RNA-seq signal are shown in parallel. The black arrows show the direction of transcription. (E) Heatmap showing enrichment of mH2A1 isoforms sites (see Fig 1A) with H3K27me3 ; from left to right, 5 equal size categories as a function of differences in

1089 H3K27me3 and H3K9me3 signals. Stars indicate significance, red and blue
1090 highlights positive and negative correlations, respectively.

1091
1092 **Fig 2. The mH2A1.1 isoform is enriched at super-enhancers.** (A) Genome
1093 browser view of ChIP-seq profiles illustrating occupancy of mH2A1 isoforms with
1094 H3K27ac and H3K4me1 histone marks on genomic regions excluding TSS. (B)
1095 Overlap of “putative” enhancers (Methods) with mH2A1 isoforms. (C) Genome
1096 browser view of ChIP-seq profiles illustrating occupancy of mH2A1 isoforms (Ab
1097 α mH2A1.1 and Ab α mH2A1) at “putative” super-enhancers (SEs). SEs were defined
1098 using the ROSE package (Methods). (D) Overlap of SEs with mH2A1 isoforms. On
1099 genome browser views, peaks and unstranded RNA-seq signal are shown in parallel.
1100 The black arrows show the direction of transcription. On venn diagrams, percentages
1101 of overlaps are given. Results of fisher exact tests are shown (p-value (p) and Odd
1102 ratio) (see Materials and Methods).

1103
1104 **Fig 3. mH2A1.1 is recruited to the transcription start site of active genes.** (A)
1105 Overlap of mH2A1 isoforms with TSSs (+/- 1kb). (B) Metagene plot of average (+/-
1106 s.d) of mH2A1 isoforms enrichment at TSSs (+/- 2 kb) categorized by gene
1107 expression levels (Methods). Colors denote gene classes as indicated. (C) Genome
1108 browser view of ChIP-seq profiles illustrating the binding of mH2A1.1 to the TSS of a
1109 transcribed gene in an open chromatin state. Peaks and unstranded RNA-seq signal
1110 are shown in parallel. The black arrows show the direction of transcription. (D)
1111 Heatmap showing peak enrichment of mH2A1 isoforms sites (see Fig 1A) at TSSs
1112 (+/- 1kb), divided into 5 equal size categories as a function of expression level
1113 (Methods). Stars indicate significance. Red and blue highlights positive and negative

correlations, respectively.(E) Metagene plot of average (+/- s.d) of mH2A1.1, H3K27ac and PolII enrichment at TSS (+/- 2kb). (F) Overlap of mH2A1 isoforms with Pol II at TSSs. On venn diagrams, percentages of overlaps are given. Results of fisher exact tests are shown (p-value (p) and Odd ratio) (see Materials and Methods).

Fig 4. mH2A1.1 activates gene expression when it binds only on their TSSs. (A) Volcano plot showing fold change of gene expression in mH2A1.1 KD compared to WT MDA-MB231 cells. Red dots represent significantly de-regulated genes with a foldchange > 1.5 and padj < 0.1. Total mH2A1.1 regulated-genes are shown. (B) Heatmap showing mH2A1 isoforms and Pol II relative enrichment around the TSS (+/- 10 kb) of mH2A1.1 KD de-regulated genes (see Fig 4A). Colour intensity reflects level of ChIP-seq enrichment. (C) Genome browser view of ChIP-seq profiles illustrating mH2A1.1 localization and genomic environment of a mH2A1.1 repressed-gene. (D) As in (C) but for a mH2A1.1 activated- gene. On genome browser views, peaks and unstranded RNA-seq signal are shown in parallel. The black arrows show the direction of transcription.

Fig 5. mH2A1.1 binds a subset of TSSs of paused genes and promotes their transcription. (A) Heatmap showing Pol II and mH2A1 isoforms enrichment around the TSS (+/- 10 kb) of transcribed genes (n=10,198) ranked by their pausing index (Methods). Colour intensity reflects level of ChIP-seq enrichment. (B) Heatmap showing correlation between mH2A1.1 peak width at TSSs (+/-1 kb) and pausing index. Genes were divided in 3 equal size categories according to their pausing index. mH2A1.1 peaks were divided in 5 categories according to their width. Stars indicate significance. Red and blue highlights positive and negative correlations,

respectively. (C) Genome browser view of ChIP-seq profiles illustrating mH2A1.1 localization on a paused gene. Peaks and unstranded RNA-seq signal are shown in parallel. The black arrows show the direction of transcription. (D) Overlap of mH2A1 isoforms sites (mH2A1.1 only and mH2A1.2 only, see Fig 1A) with paused genes (Pausing index , $PI > 2$, $n=6,821$) at their TSSs. (E) Overlap of mH2A1.1 regulated-genes with paused genes ($PI > 2$, $n=6,821$). (F) Boxplot showing pausing index of five different groups of genes, as indicated. “****” = $p\text{-value} < 2.2 \times 10^{-16}$. NS, not significant. On venn diagrams, percentages of overlaps are given. Results of fisher exact tests are shown (p-value (p) and Odd ratio) (see Materials and Methods).

Fig 6. mH2A1.1 inhibits cell migration by in part favouring expression of paused genes involved in cytoskeleton and cell adhesion in MDA-MB231 cells.

(A) Representative DIC microscopy images of WT, mH2A1.1 KD (two different siRNA) and mH2A1.2 KD MDA-MB231 cells. Scale bar = 100 μ M. (B) Immunofluorescence of Actin (up), Tubulin- α (middle) and Vimentin (down) in WT, mH2A1.1 KD and mH2A1.2 KD MDA-MB231 cells. Nuclei are stained with Hoechst. Scale bar = 20 μ M. (C) Boyden chamber assay representatives images of WT, mH2A1.1 KD and mH2A1.2 KD MDA-MB231 cells. Only migrated cells are labelled in purple. Scale bar = 150 μ M. (D) Quantification of Boyden chamber assay presented in (C). Error bar represents s.d from $n=3$ independent experiments as illustrated in (C). “*” = $p\text{-value} (p) < 0.05$, **, $p < 0.01$. (E) Overlap of paused genes ($n= 6,821$) with mH2A1.1 regulated genes related to cytoskeleton and cell adhesion (see Materials and Methods). On venn diagrams, percentages of overlaps are given. Results of fisher exact tests are shown (p-value (p) and Odd ratio) (see Materials and Methods).

1164

1165 **S1 Fig. The antibody Ab α mH2A1.1 recognizes unequivocally only the isoform**

1166 **mH2A1.1.** (A) RTqPCR on MDA-MB231 and MCF7 cells showing their relative

1167 mH2A1 isoforms mRNA expression level. Relative expressions are normalized by

1168 RPLP0 mRNA. (B) Western blot on whole cell extracts of MDA-MB231 and MCF7

1169 cells showing the better affinity of Ab α mH2A1.1 to recognize mH2A1.1 compared to

1170 Ab#37264 (Ab α mH2A1). Ab#61427 is specific to mH2A1.2. GAPDH is used as a

1171 loading control. (C) Western blot showing specific recognition of mH2A1.1 isoform by

1172 Ab α mH2A1.1 antibody. For that, HEK-293T cells were transfected with plasmids

1173 coding for Flag-mH2A1.1 (Flag1.1) or Flag-mH2A1.2 (Flag1.2) fusion overexpressed-

1174 protein. Western blot was then done with Ab α mH2A1.1, Ab#Flag and Ab#E215 (that

1175 preferentially recognizes mH2A1.2) antibodies on whole cell extracts. GAPDH is

1176 used as a loading control. (D) Immunofluorescence in HEK-293T cells showing

1177 specific recognition of mH2A1.1 isoform by Ab α mH2A1.1. (E) Western blot on ChIP

1178 extracts from HEK-293T cells overexpressing Flag1.1 or Flag1.2 showing that Ab

1179 α mH2A1.1 immunoprecipitates only mH2A1.1 isoform (Methods). Different extracts

1180 were loaded : Input fraction (Input), Non immunoprecipitated fraction (NoIP) and

1181 immunoprecipitated fraction (IP). Percentages represent percentages loaded on

1182 western blot compared to quantity used for ChIP. (F) Western blot showing that Ab

1183 α mH2A1.1 is also working in ChIP in MDA-MB231 cells on the endogenous protein.

1184 (G) As in (C), but for Ab α mH2A1 (Ab#37264) antibody showing that its antibody

1185 recognizes both isoforms but it less affine for Flag1.1 than Ab α mH2A1.1. (H) As in

1186 (G), but in immunofluorescence. (I), As in (E), but for Ab α mH2A1 (Ab#37264)

1187 antibody.

S2 Fig. (A) Whole genome spearman correlation heatmap of ChIP-seq data. Pearson coefficient correlations (PCC, r) are given. Red and blue colours denote high correlation (r close to 1) and anti-correlation (r close to -1), respectively. (B) Table showing PCCs obtained between mH2A1.1 and mH2A1 at different genomic region, as presented.

S3 Fig. Specific partial depletion of mH2A1 isoforms in MDA-MB231 cells. (A) RTqPCR showing specific partial depletion of mH2A1 isoforms mRNA by specific siRNA three days post-transfection (see Materials and Methods). (B) Western blot showing specific depletion of mH2A1 isoforms protein by specific siRNA three days post-transfection. H3 is used as a loading control. (C) Immunofluorescence showing specific partial depletion of mH2A1 isoforms by specific siRNA three days post-transfection. DNA is labelled with Hoechst. Scale bar = 10 μ m. (D) As in (A) but with a second siRNA against mH2A1.1. (E) As in (B) but with a second siRNA against mH2A1.1. GAPDH is used as a loading control. (F) RTqPCR analysis of a subset of RNAseq-defined mH2A1.1 regulated-genes. Genes are divided in three groups, as indicated. On RTqPCR, mRNA expressions are relatives to WT condition and normalized by RPLP0 mRNA. Error bars represent s.d from independent experiments ($n \geq 2$). “*” : $p < 0.05$, “***” : $p < 0.001$, NS, not significant. On western blot, mH2A1.1 and mH2A1.2 proteins are detected with Ab α mH2A1.1 and Ab#61427, respectively. Quantifications are showed, normalized by protein loading control.

S4 Fig. (A) mH2A1 and mH2A1.1 binding at genomic regions selected based on ChIP-sequencing. Localisation of primers used for ChIP-qPCR are shown in red. (B) Occupancy of mH2A1 isoforms (left part : Ab α mH2A1.1 ; right part : Ab α mH2A1) analysed by ChIP-qPCR in control cells (WT) and cells partially deficient for

1213 mH2A1.1 using two different siRNA (mH2A1.1 KD #1 and mH2A1.1 KD #2). Error
1214 bars represent +s.d from independent experiments (n>=2).

1215 **S5 Fig. Levels of H3K27me3 and H3K9me3 are anti-correlated on common**
1216 **H3K27me3/H3K9me3 peaks.** (A) Boxplots showing H3K27me3 and H3K9me3
1217 enrichment levels on H3K27me3/H3K9me3 common peaks. Peaks were divided into
1218 5 equal size categories according to the level of H3K27me3, as mentioned. (B)
1219 Histogram showing proportions of heterochromatin genomic localization, as
1220 mentioned. Peaks were divided into 5 equal size categories according to ratio
1221 between H3K27me3 and H3K9me3, as mentioned.

1222 **S6 Fig. The mH2A1.1 isoform binds to TSSs in open chromatin state whereas**
1223 **mH2A1.2 binds to TSSs in closed chromatin state.** (A) TSS (+/- 1kb) centred
1224 spearman correlation heatmap of ChIP-seq data. Pearson coefficient correlations
1225 (PCC, r) are given. Red and blue colours denote high correlation (r close to 1) and
1226 anti-correlation (r close to -1), respectively. (B) Overlap of mH2A1 isoforms sites
1227 (mH2A1.1 only and mH2A1.2 only, see Fig. 1a) with H3K4me3 and Pol II at TSS (+/-
1228 1 kb). (C) As in (B), but with H3K9me3 and H3K27me3 histone marks. Results of
1229 fisher exact tests are shown (p-value (p) and Odd ratio) (see Materials and Methods).

1230 **S7 Fig. The mH2A1.1 isoform binds the TSSs of transcribed genes.** (A) Boxplots
1231 of mH2A1 isoforms levels and Pol II at TSS (+/- 1kb) categorized by gene expression
1232 levels (see Materials and Methods). Colors denote gene classes, as indicated. "****"
1233 p-value < 2.2x10⁻¹⁶ (see Materials and Methods). (B) Metagene plot of average (+/-
1234 s.d) of mH2A1 isoforms enrichment from TSS to TES (+/- 2 kb) categorized by gene
1235 expression levels (Methods). Colors denote gene classes, as indicated. (C) Genome
1236 browser view of ChIP-seq profiles illustrating occupancy of mH2A1 isoforms on a not
1237 expressed gene. (D) As in (C) but for a highly expressed gene. (E) Heatmap showing

peak enrichment of Pol II and histone marks at TSS (+/- 1kb) divided into 5 equal size categories as a function of expression level (Methods). Stars indicate significance. Red highlights positive and blue indicates negative correlations. (F) TSS-centred spearman correlation heatmap of ChIP-seq data. Pearson coefficient correlations (PCC, r) are given. Red and blue colours denote high correlation (r close to 1) and anti-correlation (r close to -1), respectively. On genome browser views, peaks and unstranded RNA-seq signal are shown in parallel. The black arrows show the direction of transcription.

S8 Fig. The mH2A1.1 isoform regulates expression of active genes. (A) Boxplot comparing gene expression of three groups of genes (as indicated) between WT and mH2A1.1 KD cells. (B) Pie chart showing proportion of mH2A1.1 regulated-genes categorized by gene expression levels in WT cells (see Materials and Methods). Colors denote gene classes, as indicated. Results of fisher exact tests are shown (p-value (p) and Odd ratio) (see Materials and Methods). (C) Boxplot showing mH2A1 isoforms occupancy levels, Pol II and histone marks at TSS on mH2A1.1 KD regulated genes and not affected genes, as indicated. On boxplots, p-value are shown, “****” = p -value $< 2.2 \times 10^{-16}$; NS, not significant (see Materials and Methods).

S9 Fig. The recruitment of mH2A1.1 differs between mH2A1.1-activated and repressed genes. (A) Metagene plot of average (+/- sd) of mH2A1 isoforms levels and Pol II from TSS to TES (+/- 2 kb) on mH2A1.1 regulated-genes. (B) Heatmap showing correlation between Pol II peak width at TSS (+/-1 kb) and pausing index. Genes were divided in 3 equal size categories according to their pausing index. Pol II

peaks were divided in 5 categories according to their width. Stars indicate significance. Red and blue highlights positive and negative correlations, respectively.

S10 Fig. The isoform mH2A1.1 modulates expression of genes involved in cell cycle, DNA repair and cell shape. (A) List of gene ontology (GO) terms for mH2A1.1 activated-genes. The most significantly regulated ontologies were determined by adjusted p-value and are shown in three different classes, Biological Process (upper graph), Molecular function (middle graph) and Cellular Component (lower graph). A full list of enriched GO terms is provided in S4 Table. (B) As in (A) but for mH2A1.1 repressed-genes.

Supporting information legends

S1 Table. List of antibodies used for western blot, immunofluorescence, and ChIP.

S2 Table. Summary of ChIP-seq and RNA-seq.

S3 Table. List of mH2A1.1-regulated genes.

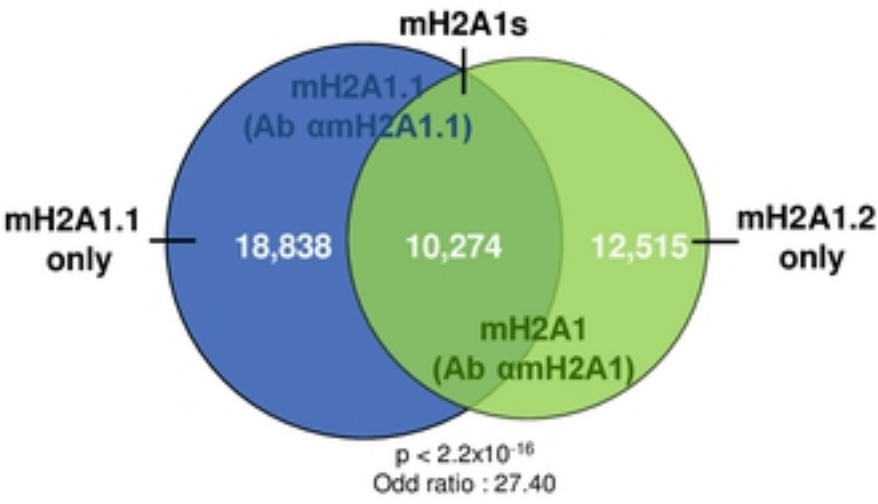
S4 Table. List of GO terms related to mH2A1.1-regulated genes.

S5 Table. Sequences used for mH2A1.1 specific antibody production and siRNAs.

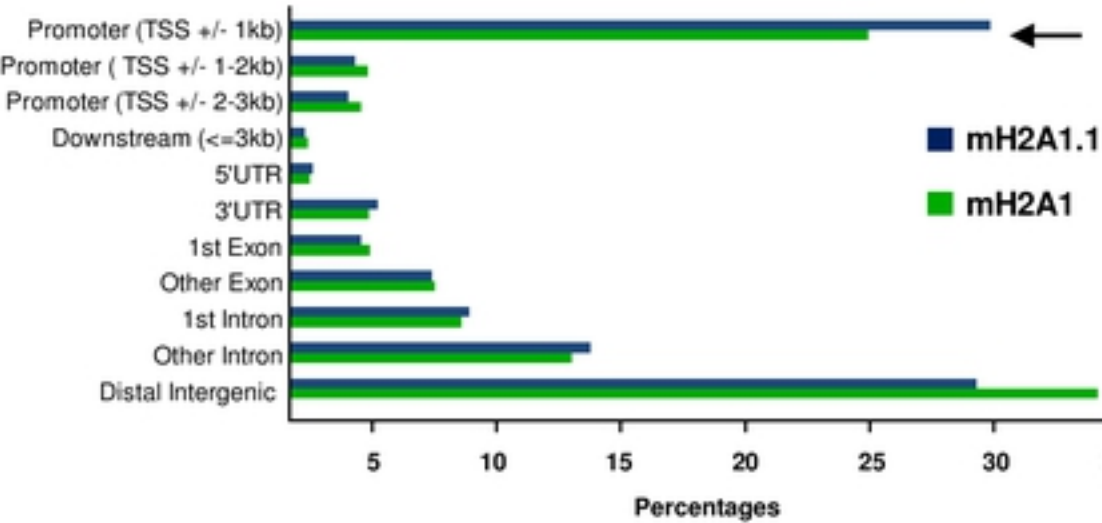
S6 Table. List of primers used for RTqPCR.

S7 Table. List of ChIPqPCR primers used for ChIPqPCR.

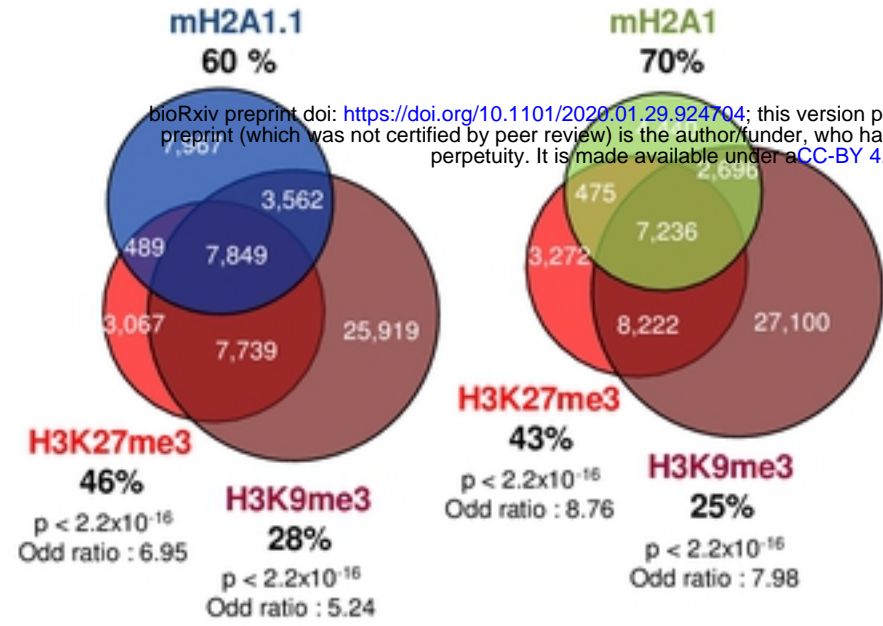
Fig 1
A



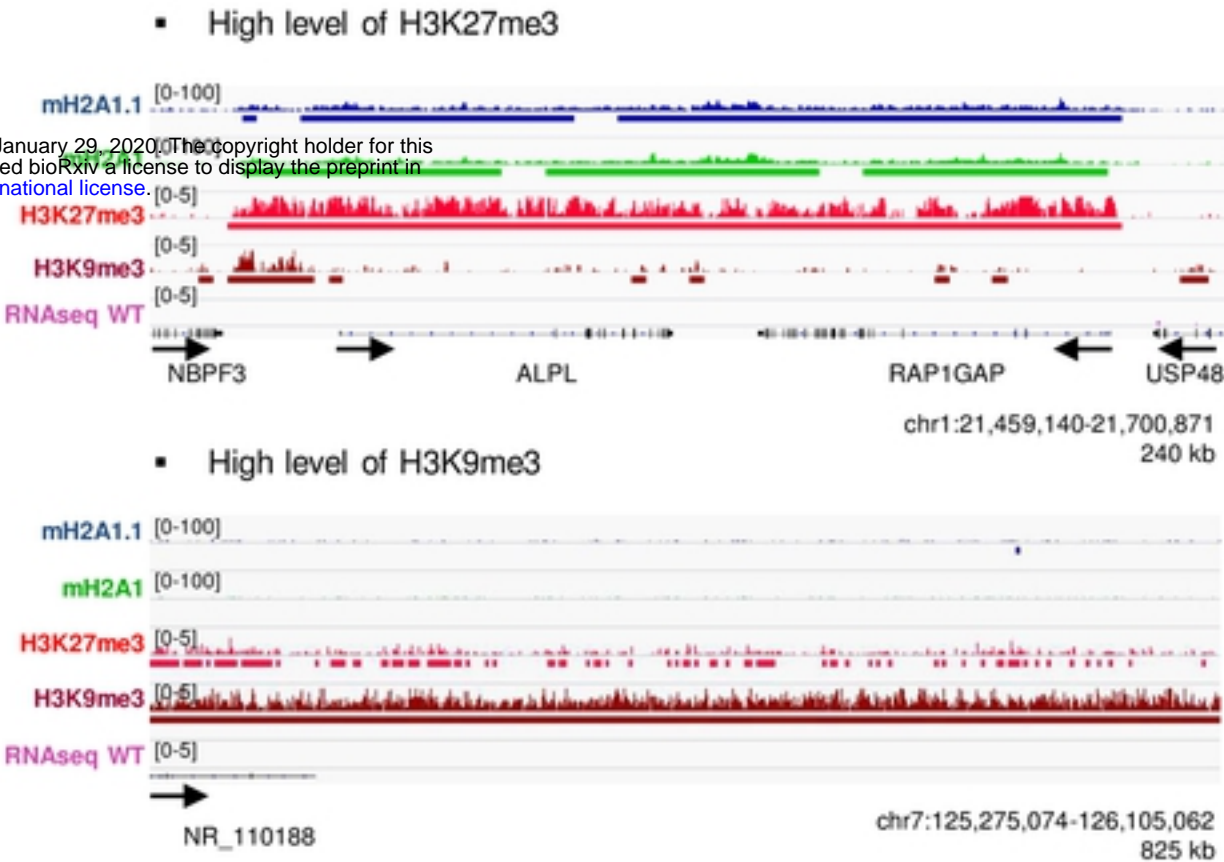
B



C



D



E

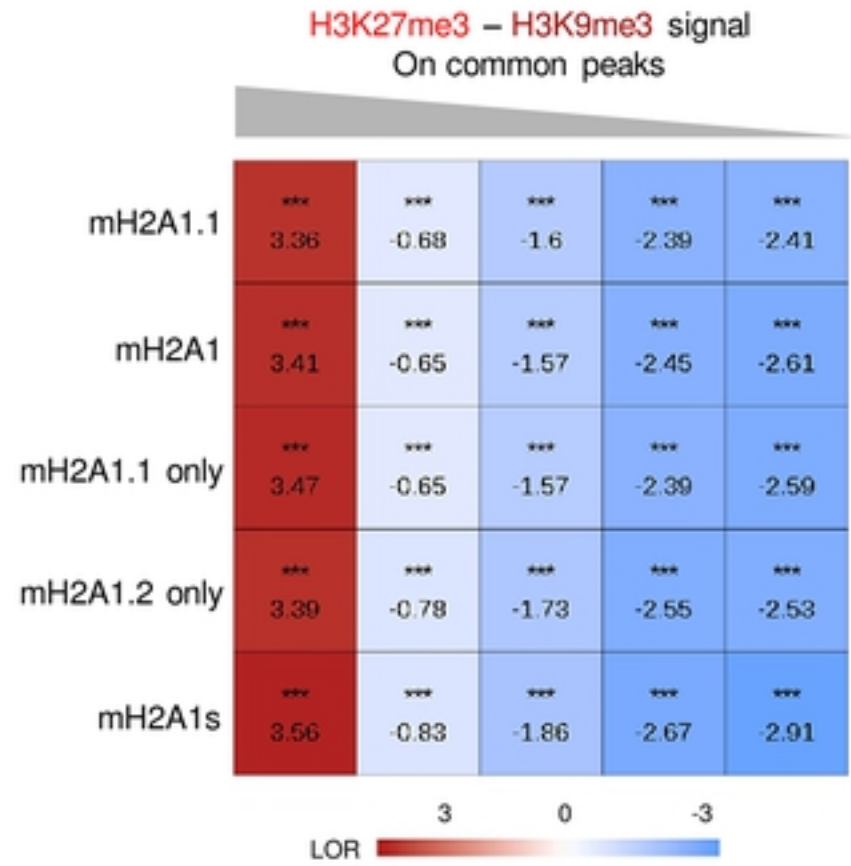
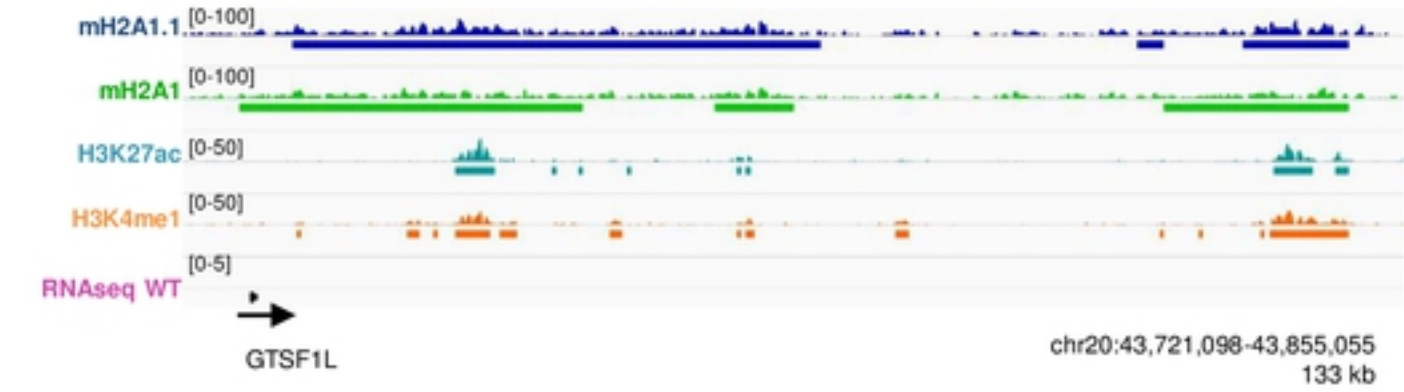
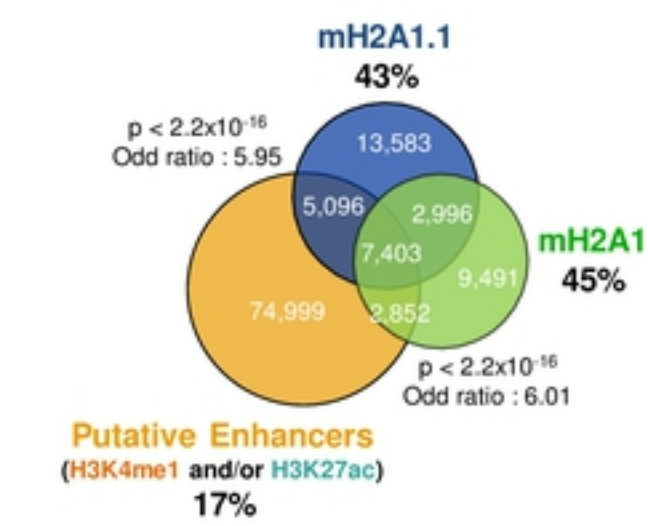


Fig 2

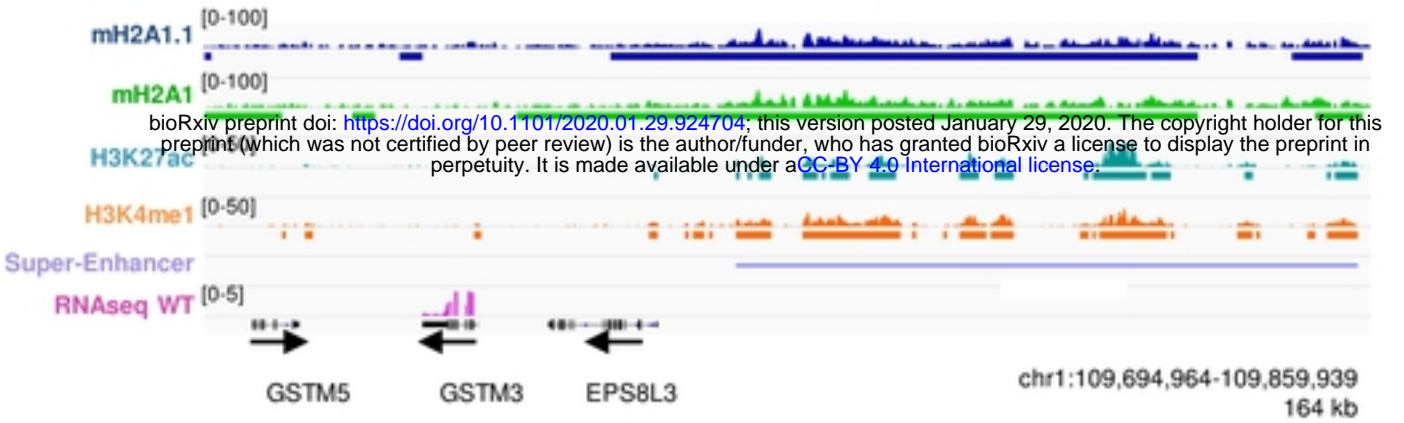
A



B



C



D

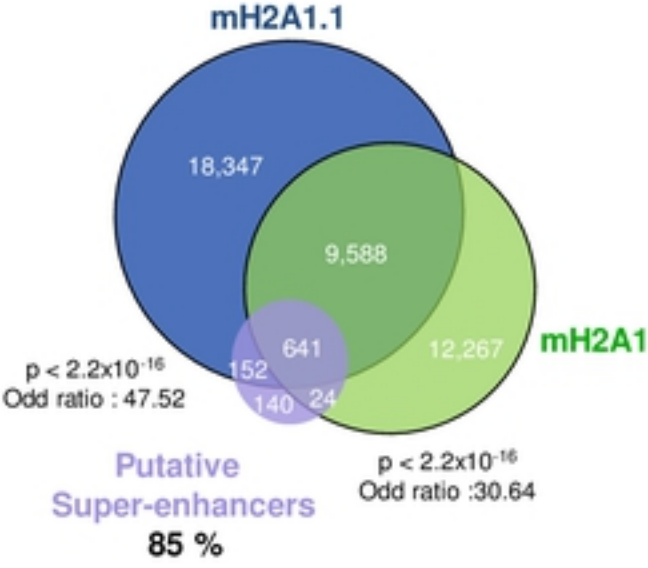
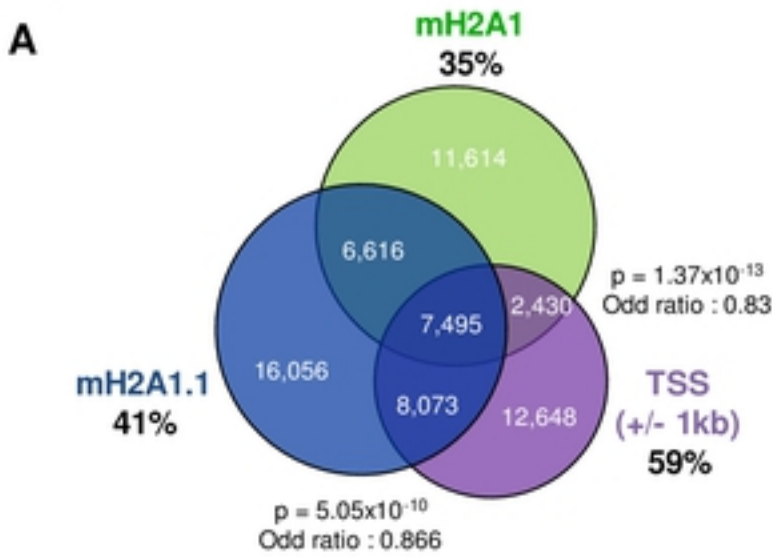
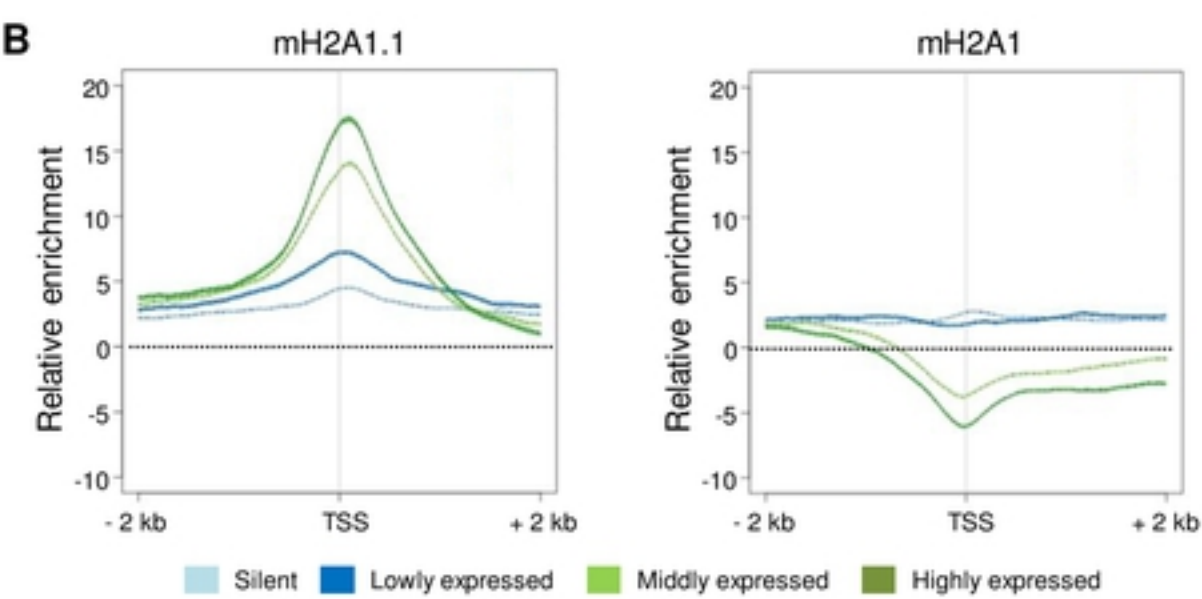


Fig 3

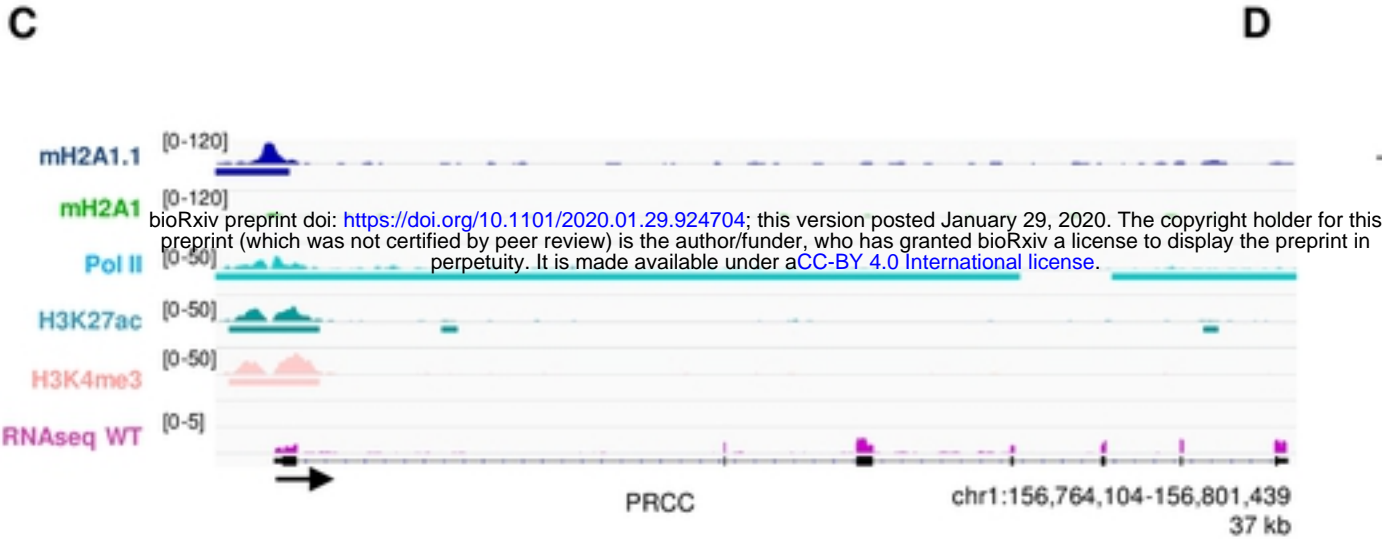
A



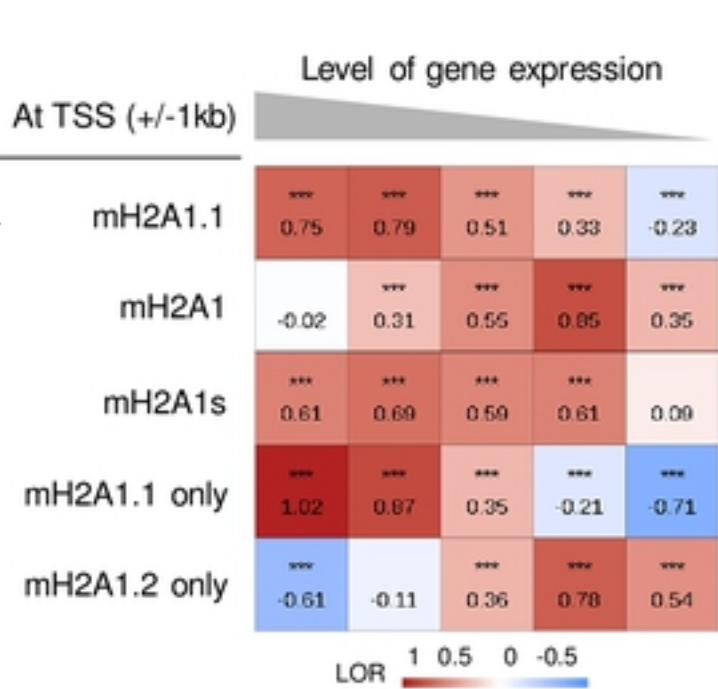
B



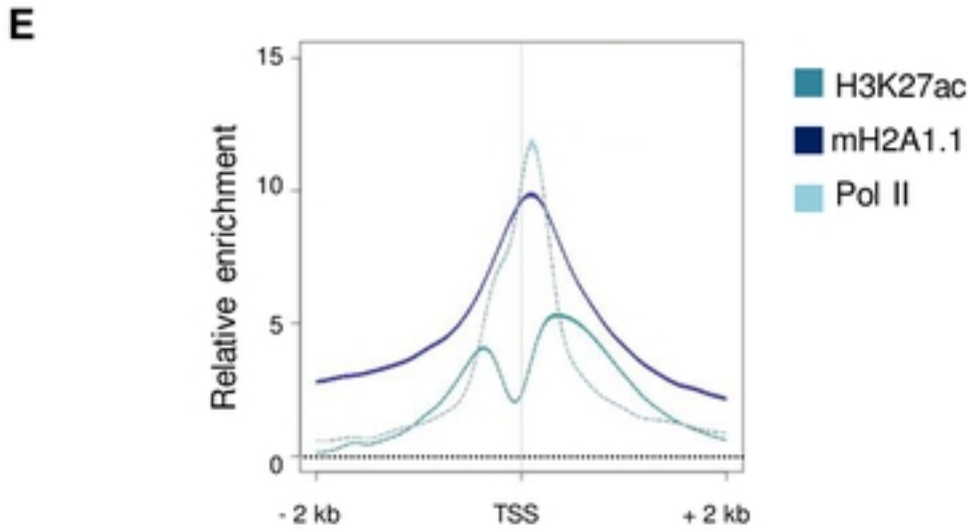
C



D



E



F

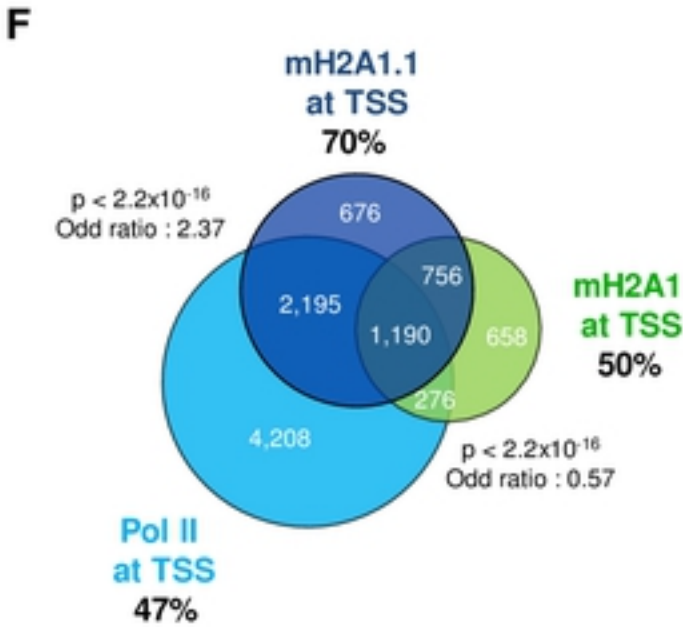


Fig 4

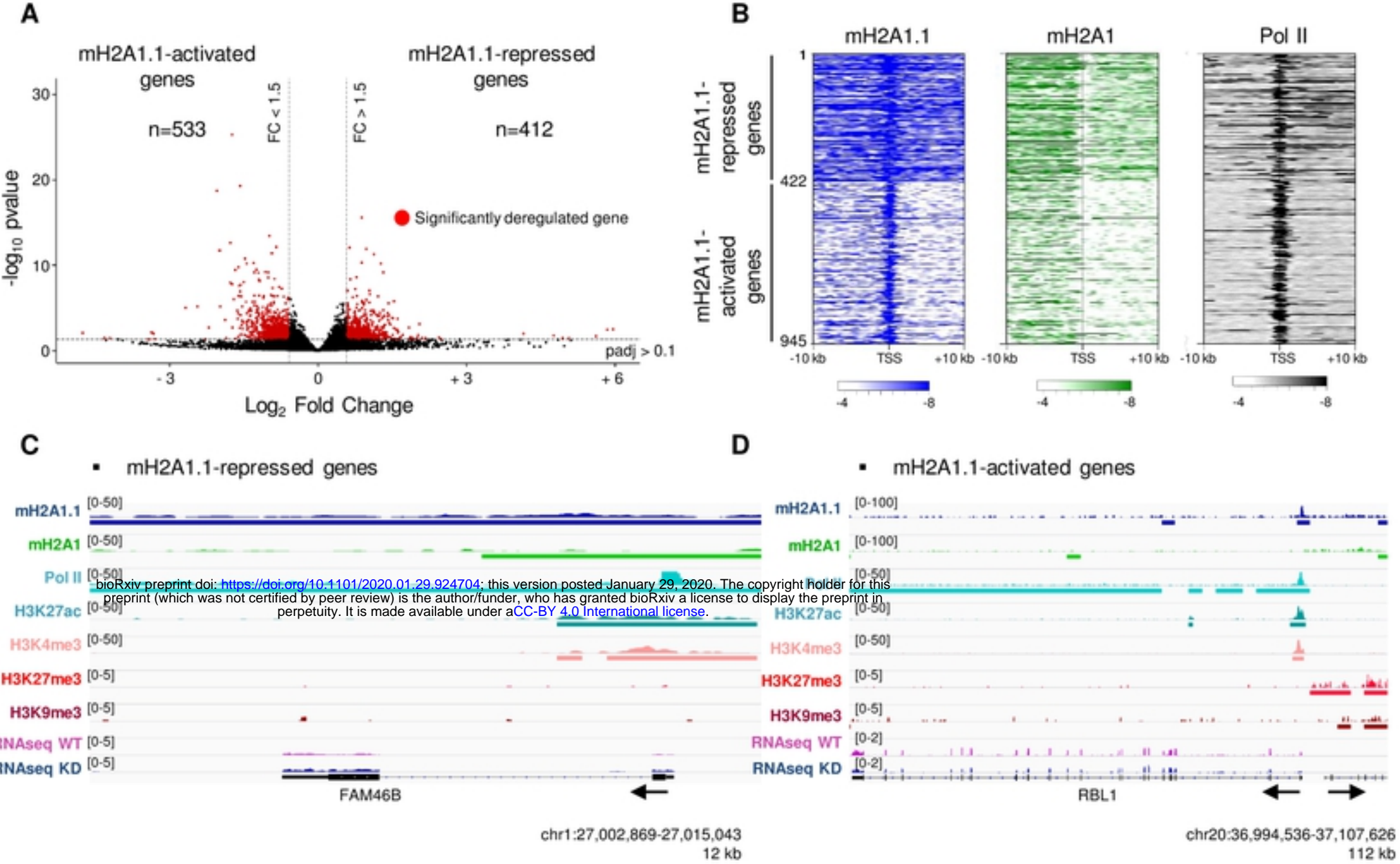


Fig 5

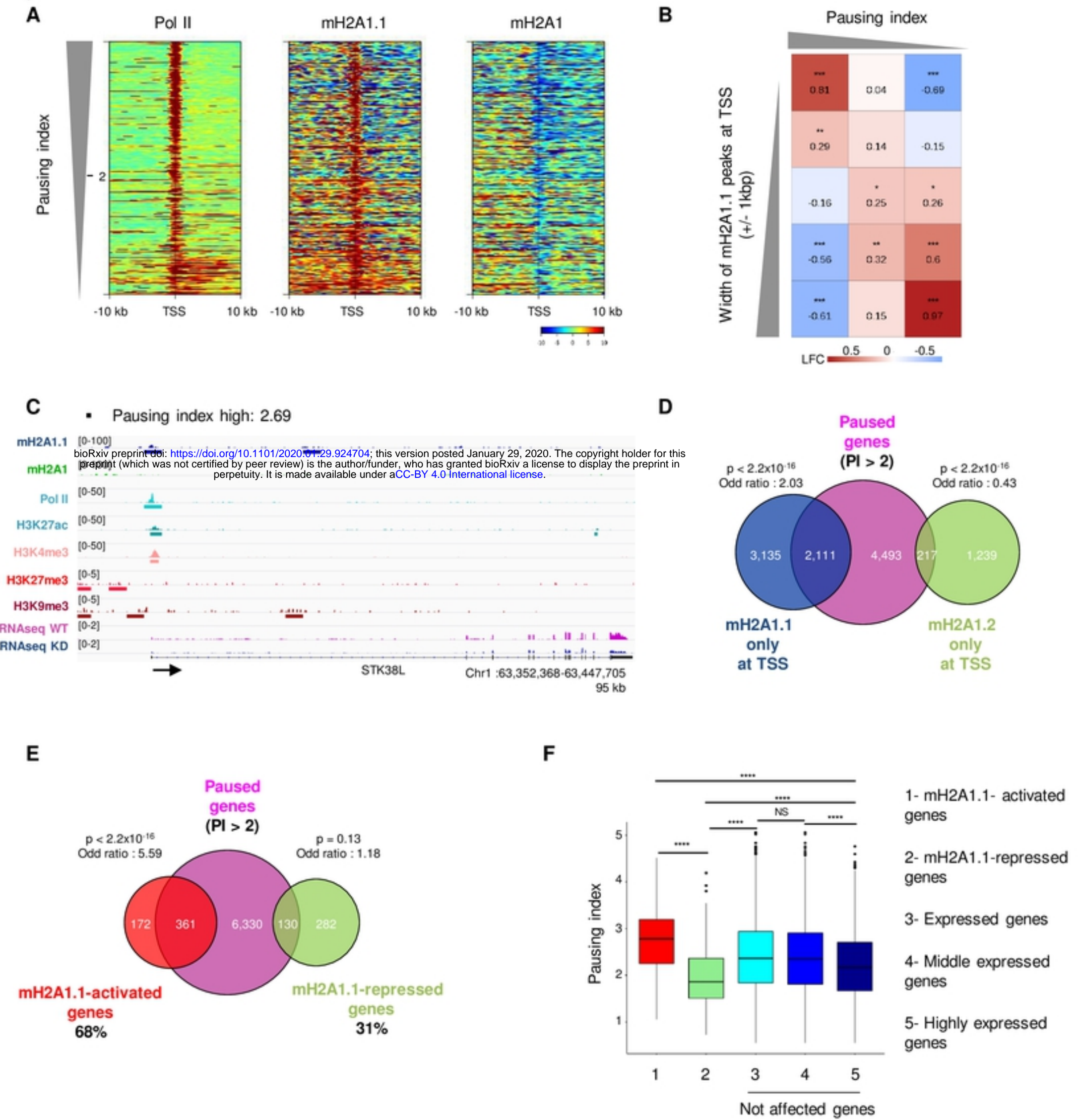
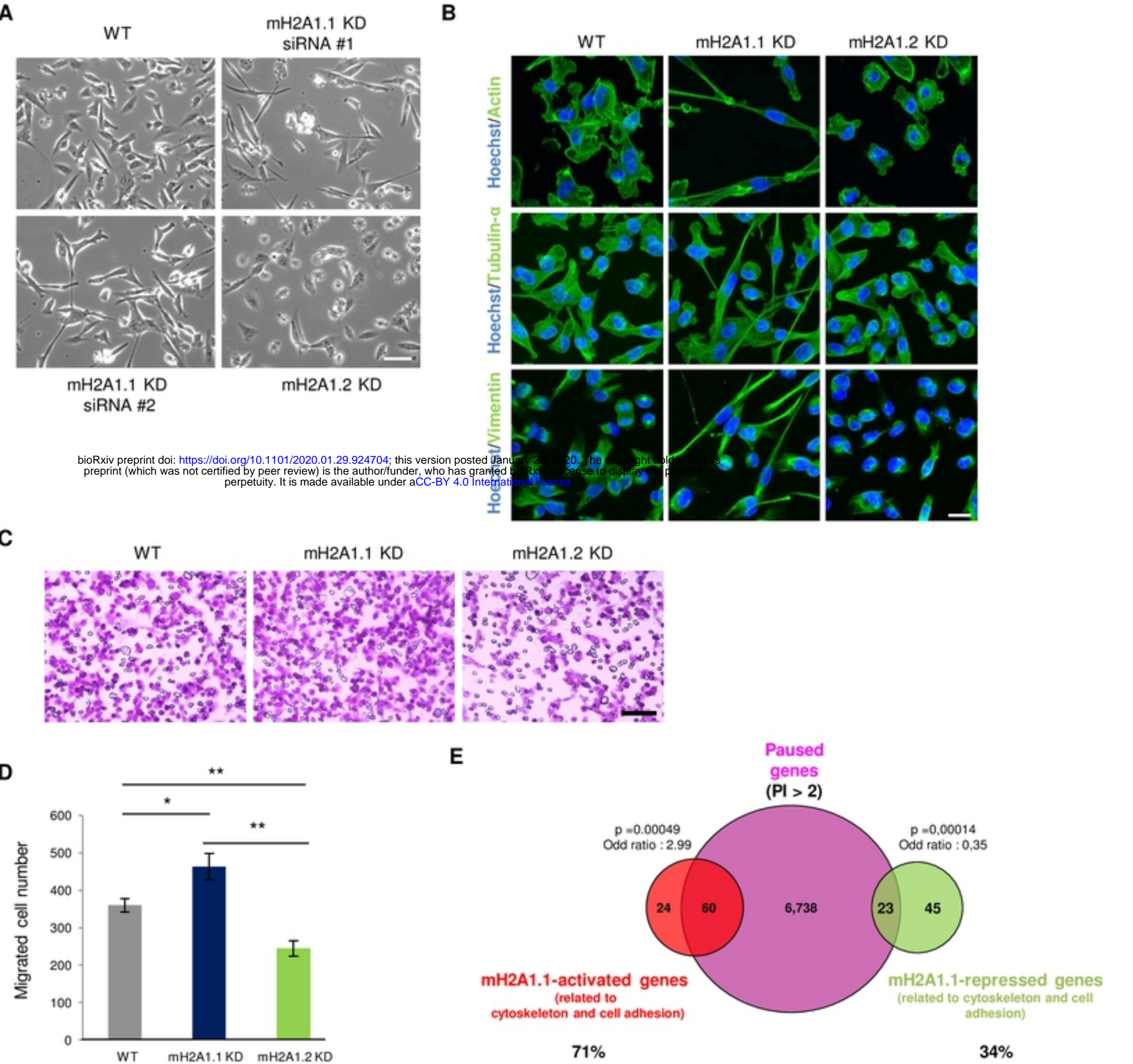
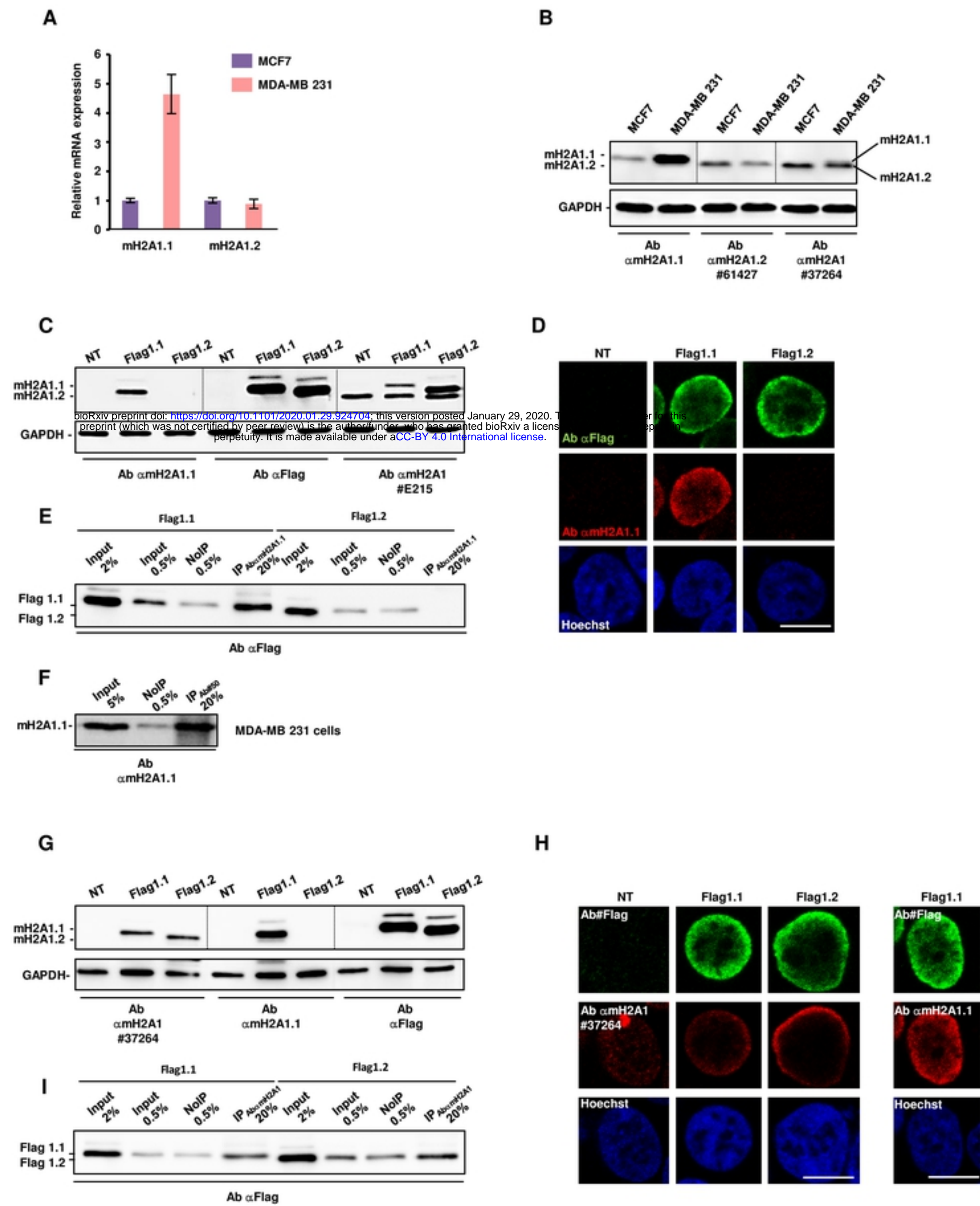
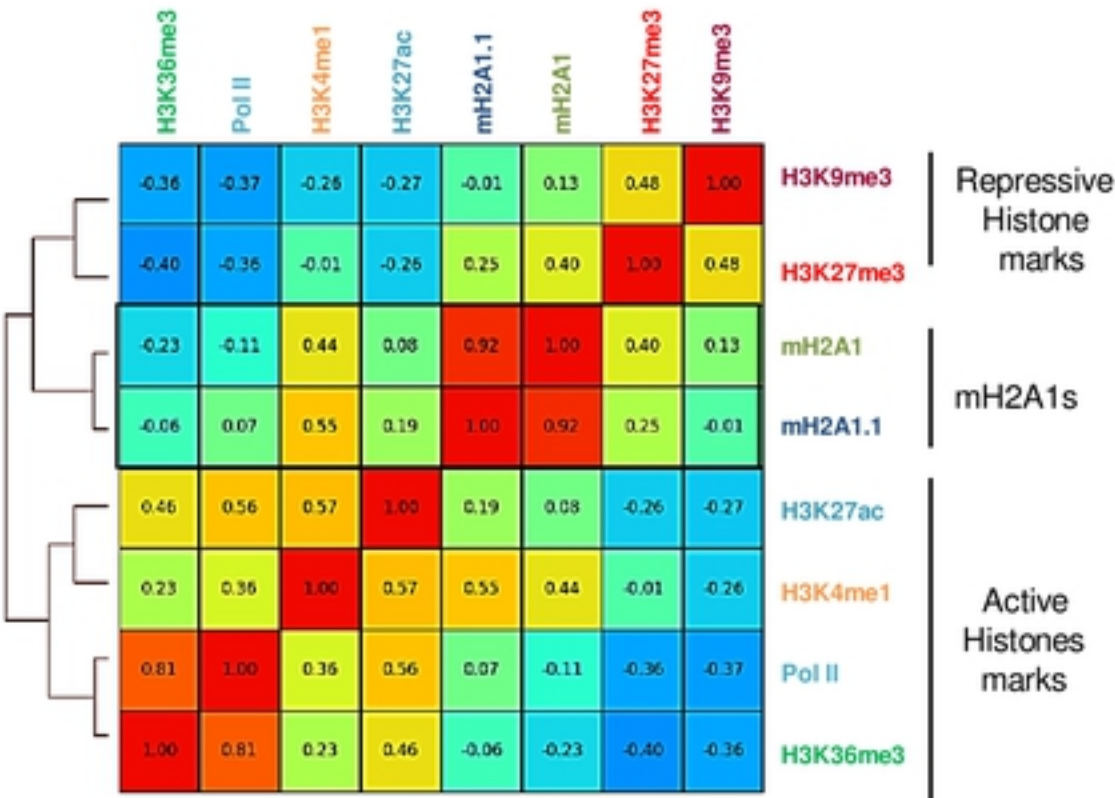


Fig 6





A

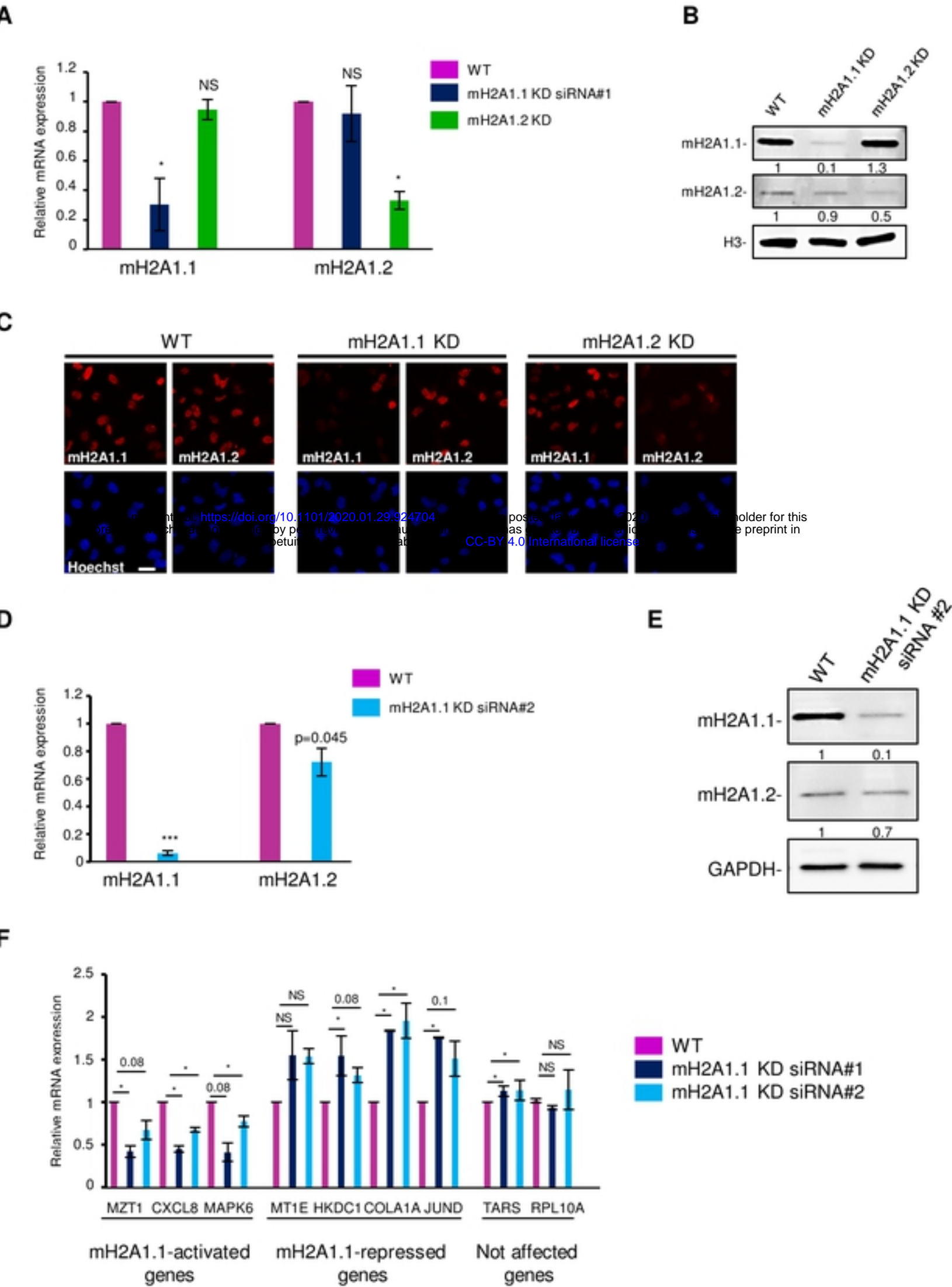


bioRxiv preprint doi: <https://doi.org/10.1101/2020.01.29.924704>; this version posted January 29, 2020. The copyright holder for this preprint (which was not certified by peer review) is the author/funder, who has granted bioRxiv a license to display the preprint in perpetuity. It is made available under aCC-BY 4.0 International license.

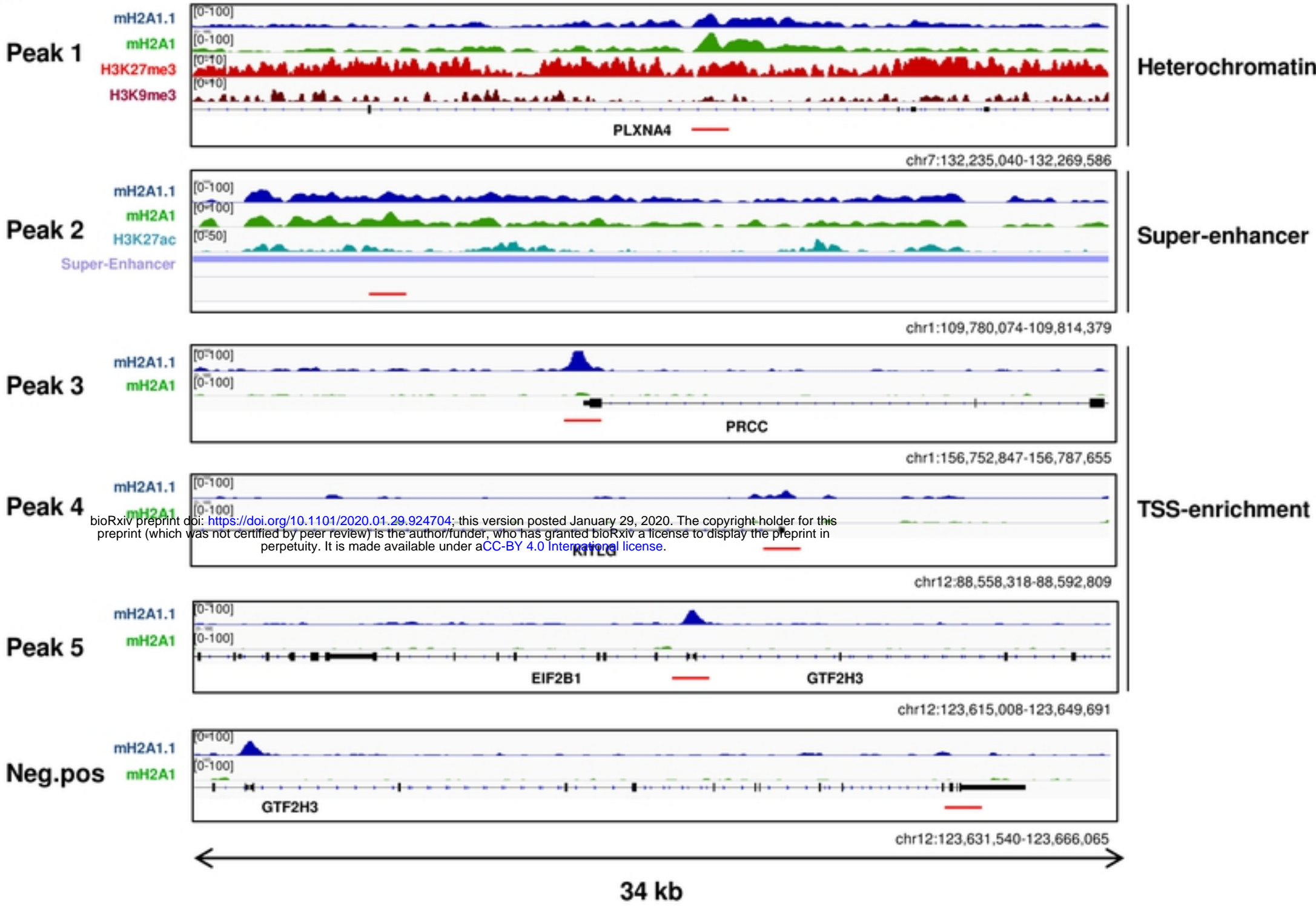
B

Genomic regions	PCC between mH2A1.1 and mH2A1
Heterochromatin	0.94
Enhancer	0.80
TSS +/- 1kb	0.41
TSS	-0.07

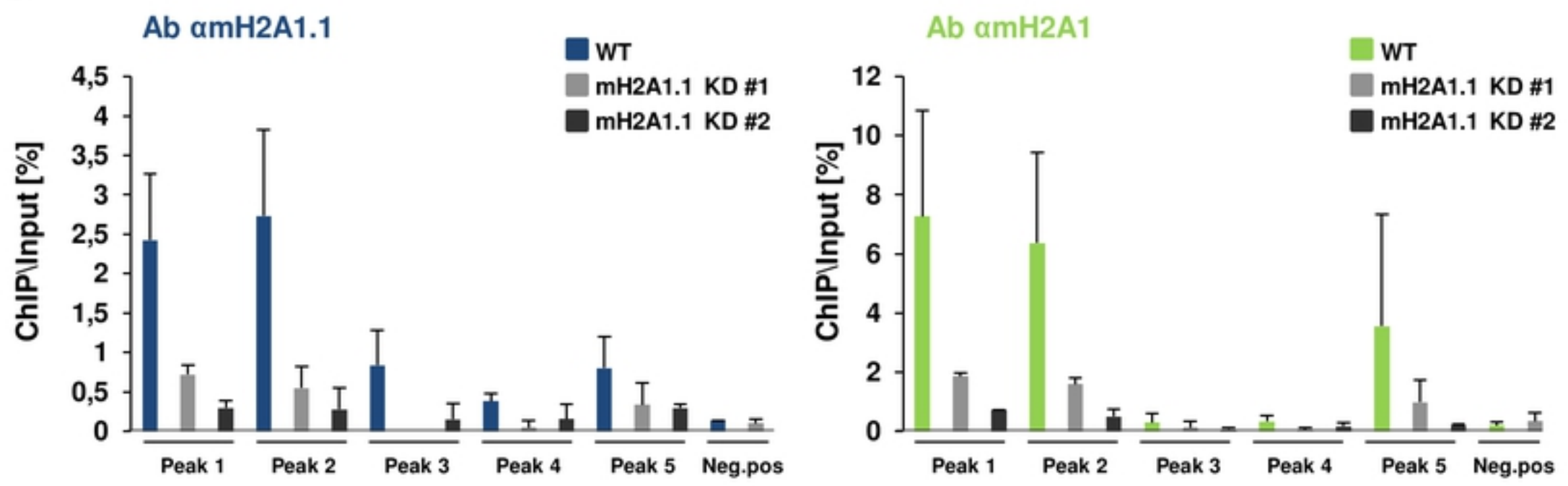
S3_Fig



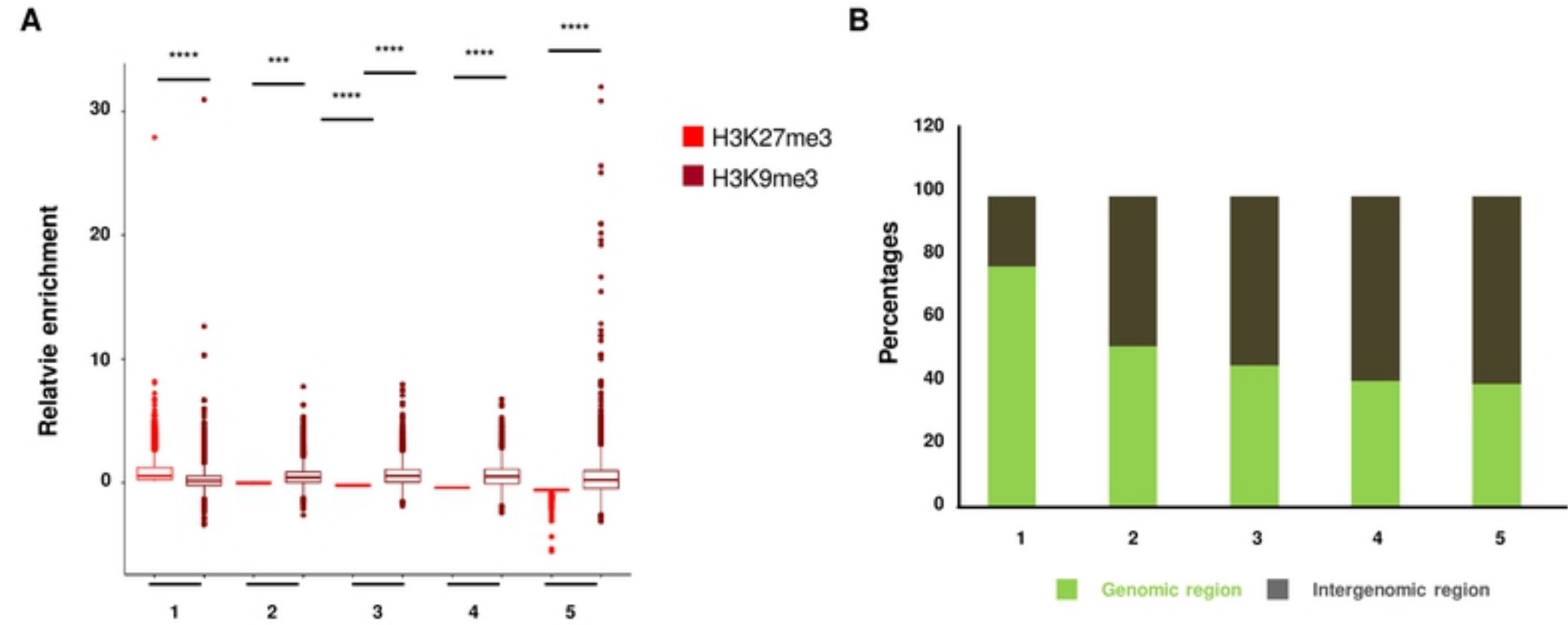
S4_Fig
A



B



S5_Fig



bioRxiv preprint doi: <https://doi.org/10.1101/2020.01.29.924704>; this version posted January 29, 2020. The copyright holder for this preprint (which was not certified by peer review) is the author/funder, who has granted bioRxiv a license to display the preprint in perpetuity. It is made available under aCC-BY 4.0 International license.

1 : Very high level of H3K27me3

2 : High level of H3K27me3

3 : Middle level of H3K27me3

4 : Low level of H3K27me3

5 : Very low level of H3K27me3

1 : Very high ratio of H3K27me3/H3K9me3

2 : High ratio of H3K27me3/H3K9me3

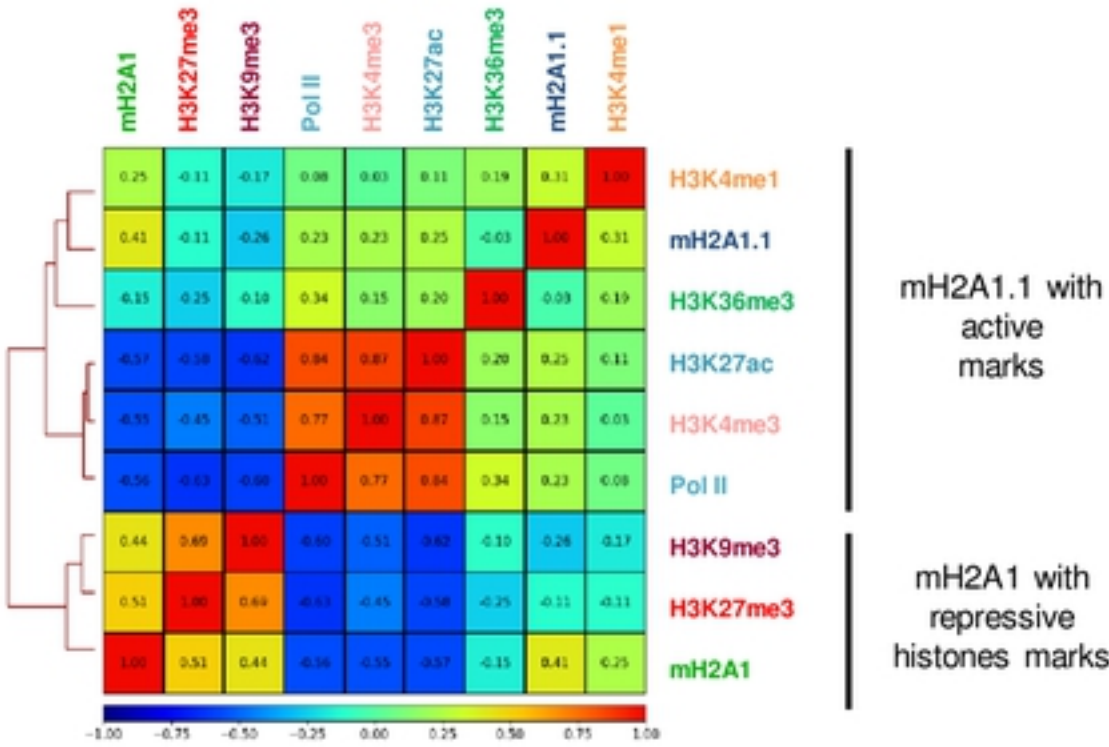
3 : Middle ratio of H3K27me3/H3K9me3

4 : Low ratio of H3K27me3/H3K9me3

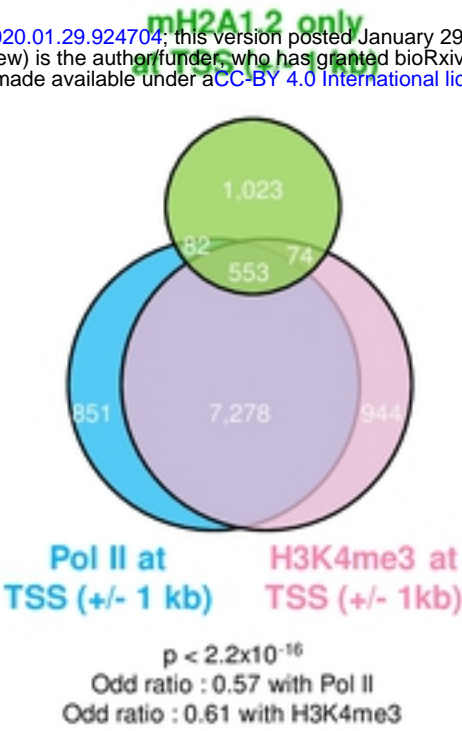
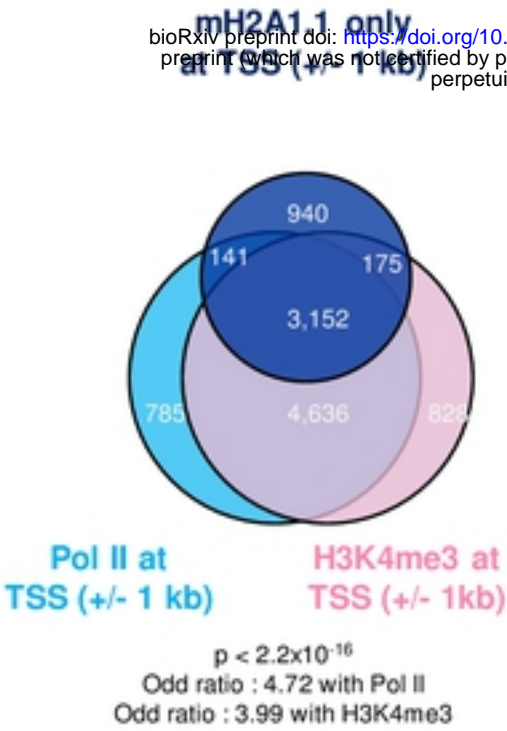
5 : Very low ratio of H3K27me3/H3K9me3

S6_Fig

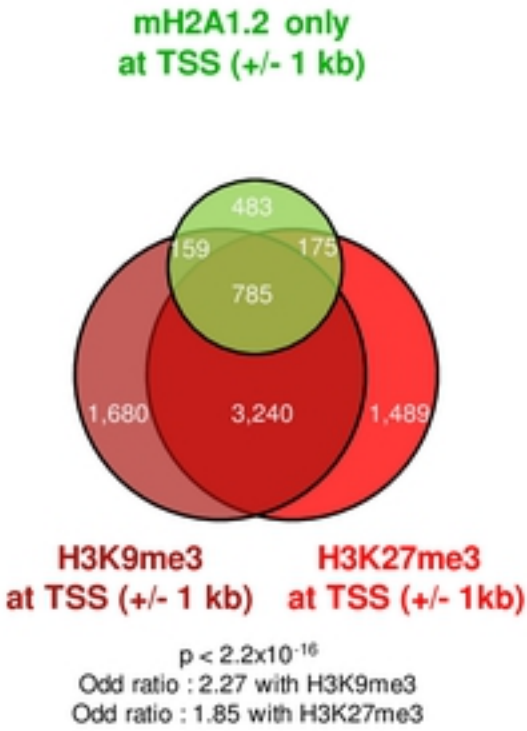
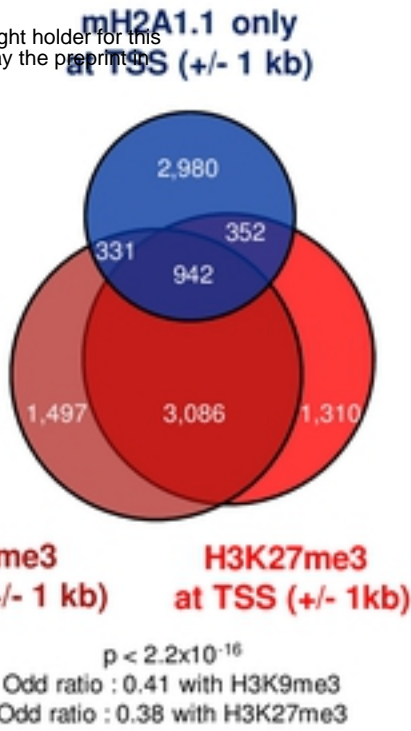
A

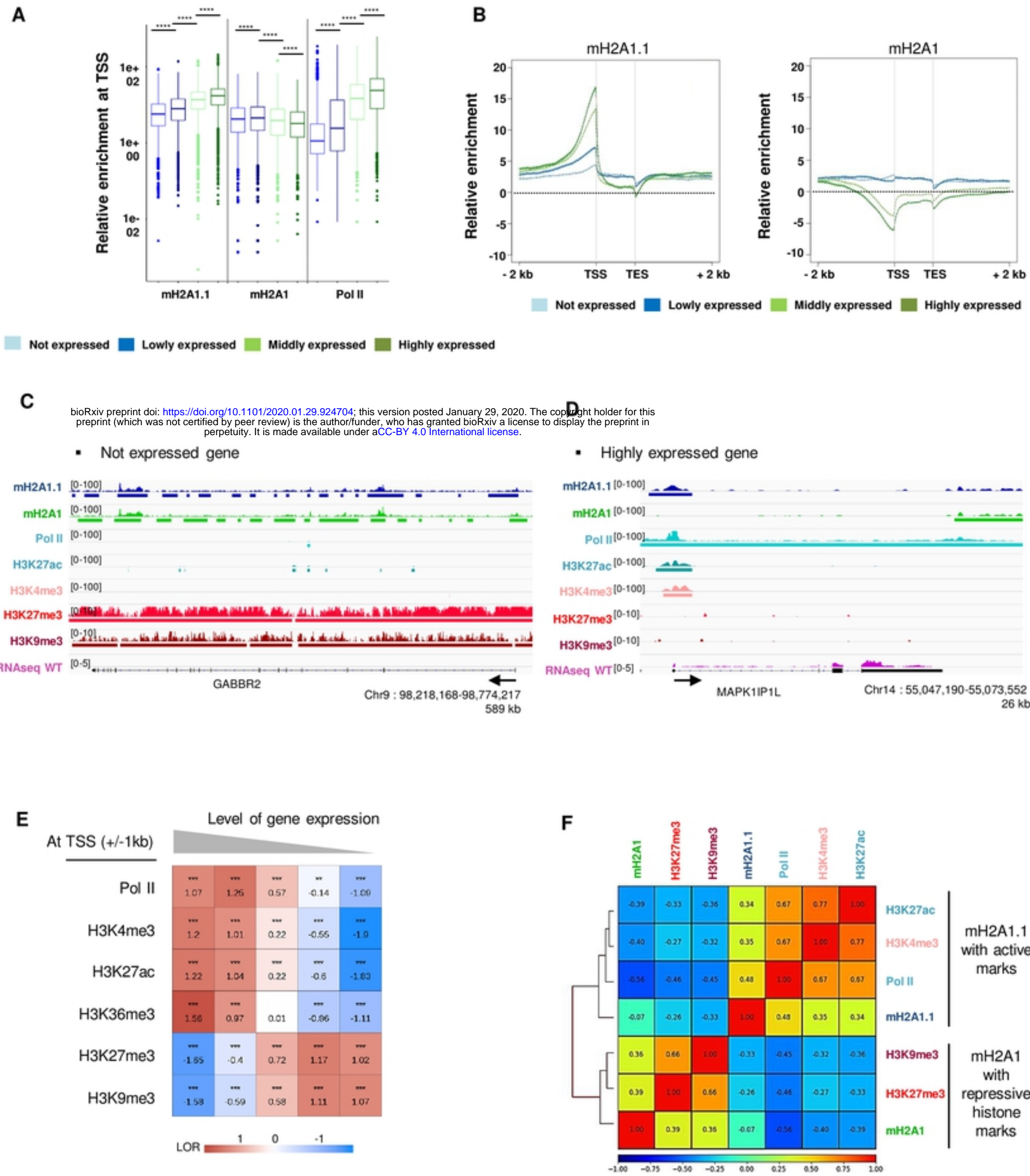


B



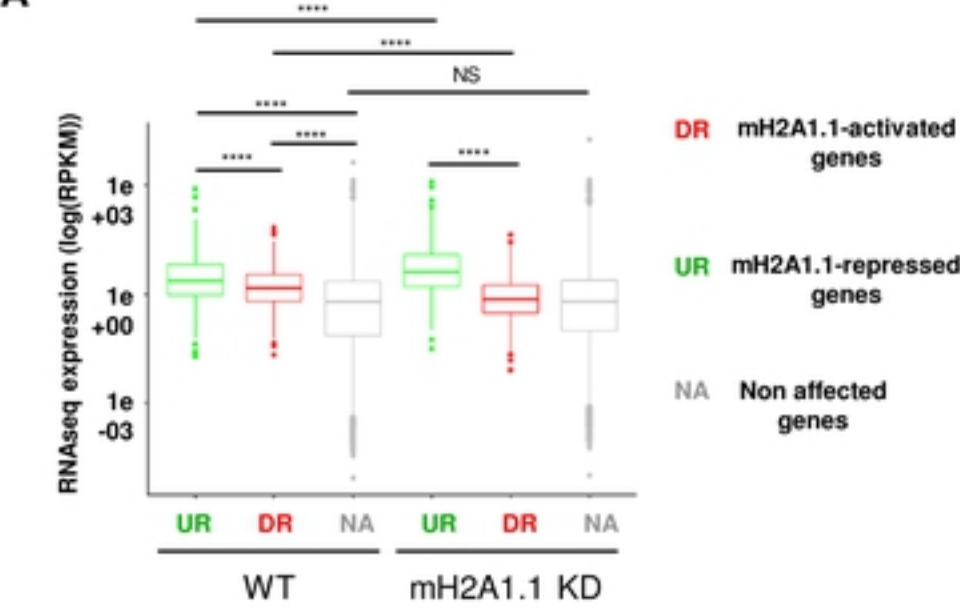
C



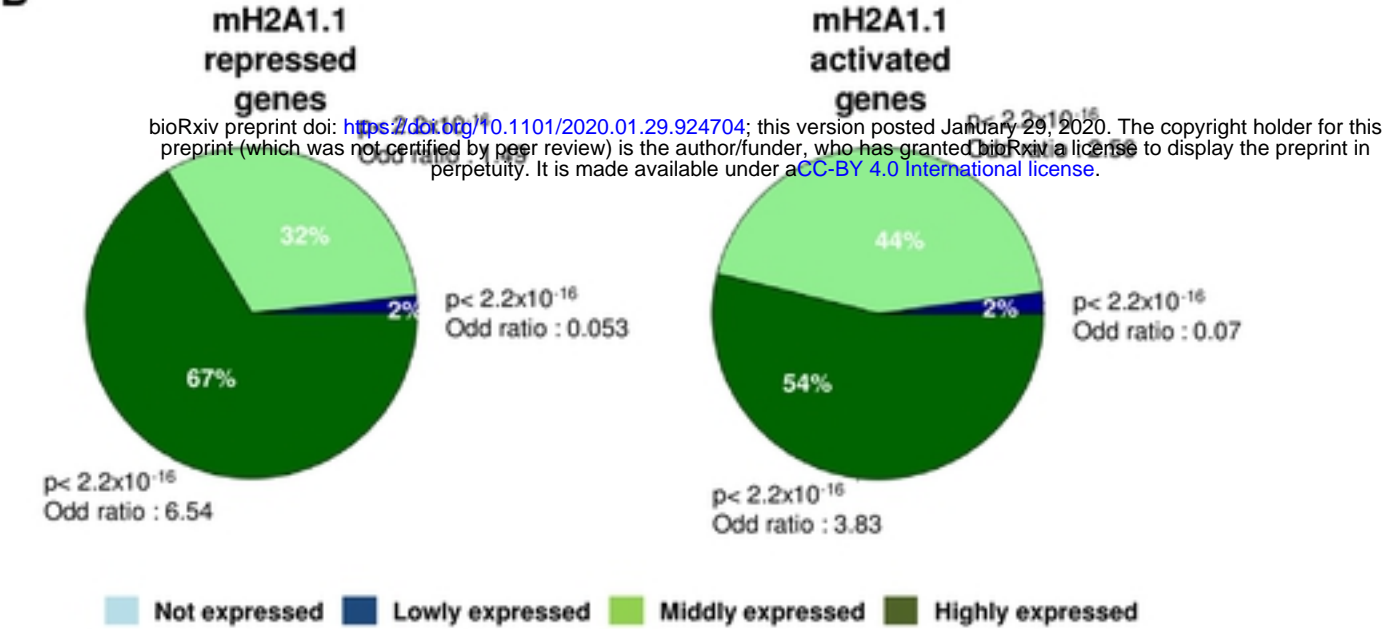


S8_Fig

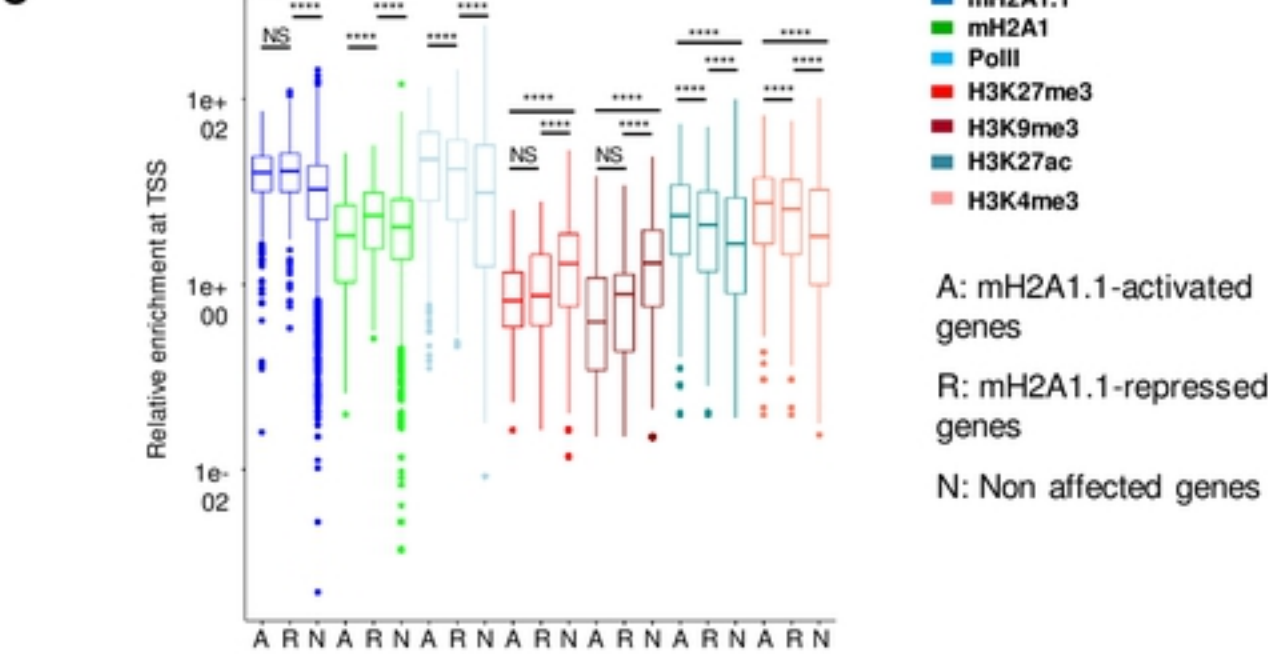
A



B

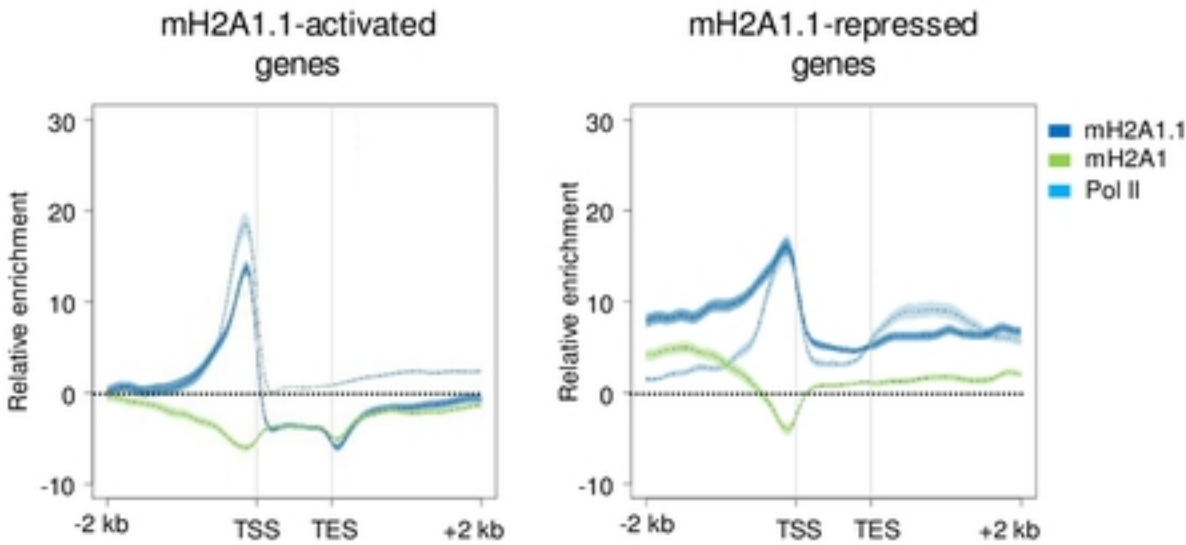


C

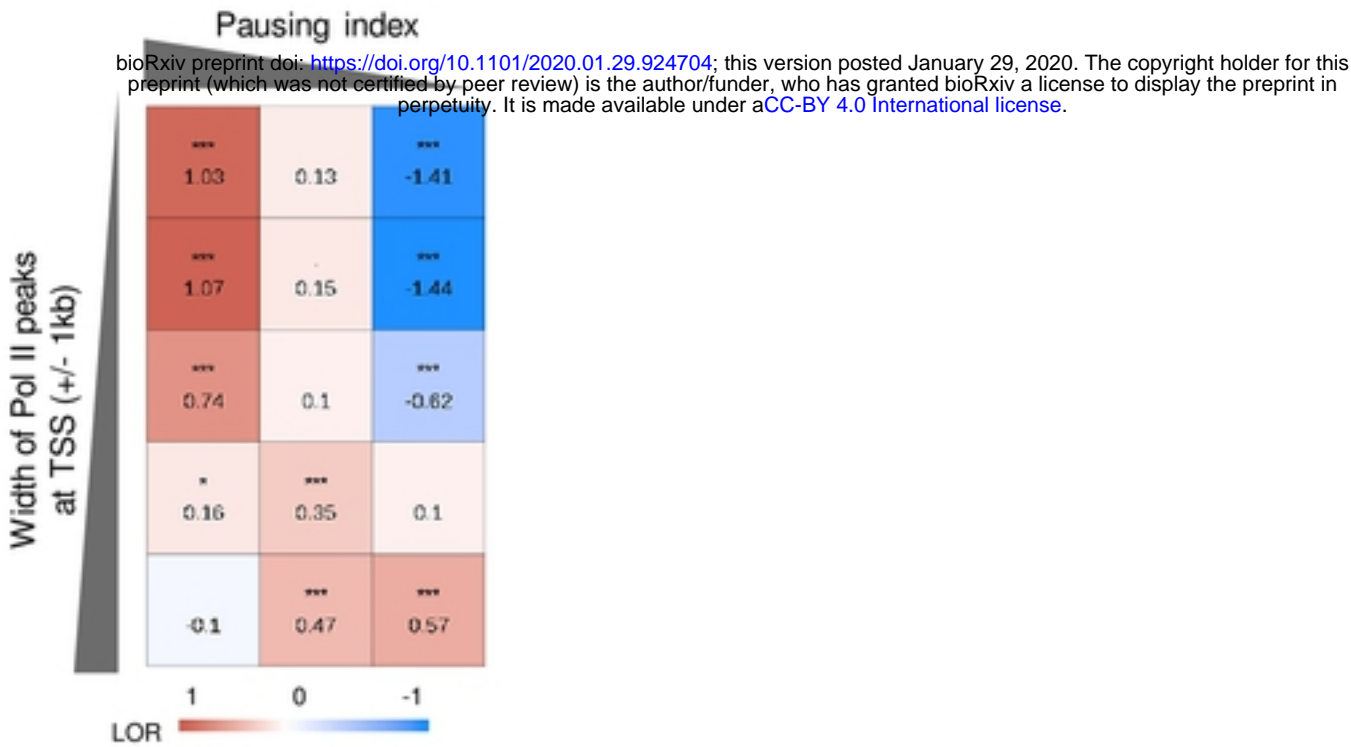


S9_Fig

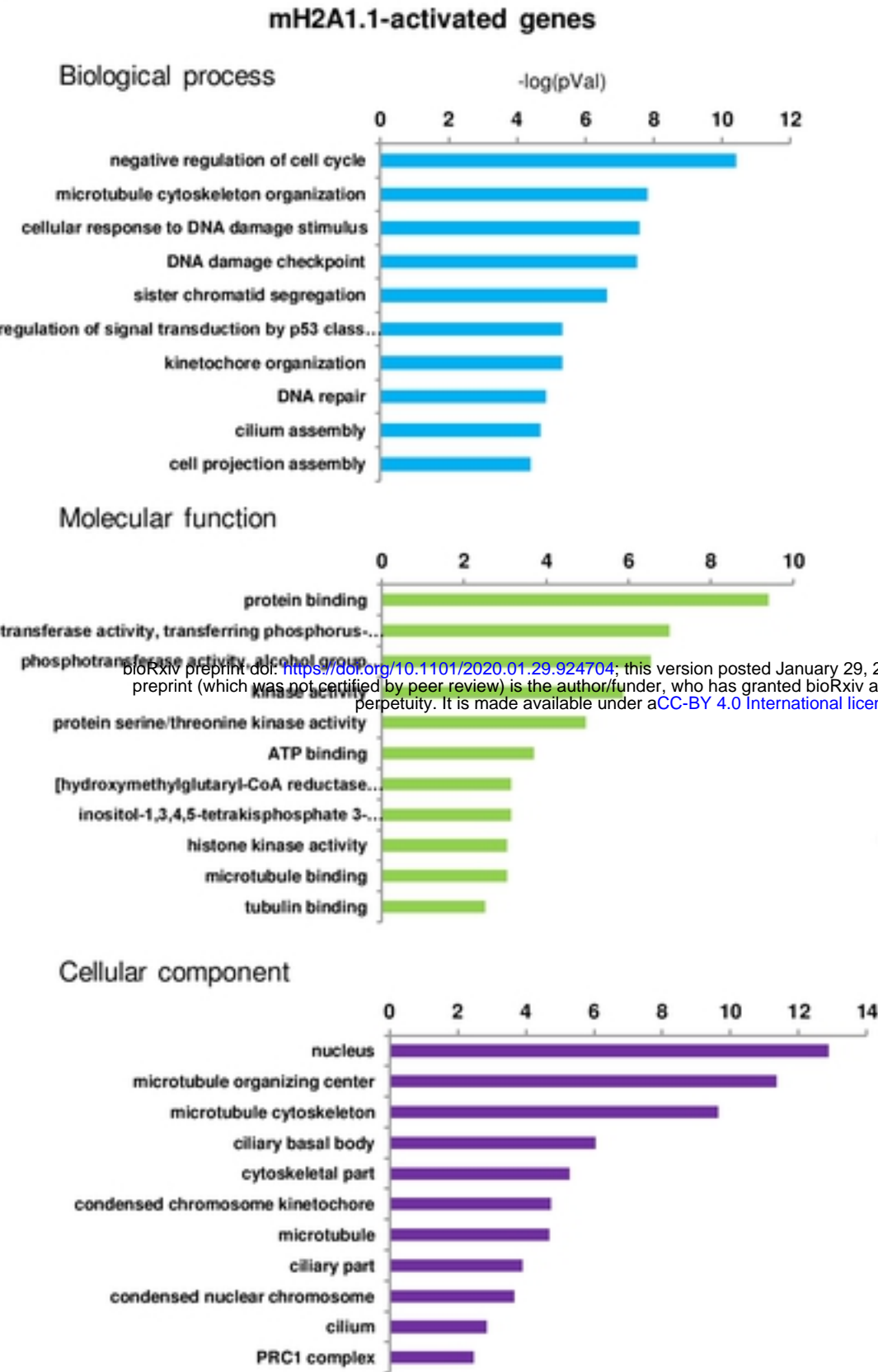
A



B



A



B

